



Universidad Nacional Autónoma de México

Instituto de Ciencias Físicas

PROTOCOLO DE INVESTIGACIÓN

TÍTULO DEL PROYECTO:

Non-linear modelling of Interacting Dark Energy theories for structure formation.

PRESENTA:

MSc. Gabriel Karim Miranda Carrion

Supervisor:

Dr. Juan Carlos Hidalgo Cuéllar

Instituto de Ciencias Físicas, Universidad Nacional Autónoma de México, Cuernavaca, México.

Co-supervisora:

Dr. Alkistis Pourtsidou

Institute for Astronomy, The University of Edinburgh, Royal Observatory, Edimburgo, Reino Unido.

Colaboradores:

Dr. Pedro Carrilho

Institute for Astronomy, The University of Edinburgh, Royal Observatory, Edimburgo, Reino Unido.

Dr. Benjamin Bose

Institute for Astronomy, The University of Edinburgh, Royal Observatory, Edimburgo, Reino Unido.

Dr. Alessio Spurio Mancini

University College London, Department of Space and Climate Physics, Londres, Reino Unido.

Cuernavaca, Morelos, 1/Noviembre/2022

Contents

List of Figures

1	Main goal	1
2	Introduction	2
3	Precedents	4
3.1	Background cosmology	4
3.2	Cosmological Perturbation Theory	6
3.2.1	Linear regime	7
3.2.2	Non-linear regime	8
3.2.3	Power spectrum	11
3.3	Halo model	13
3.3.1	Halo model reaction	16
3.4	Full spectra	18
3.4.1	Presence of Neutrinos	18
3.4.2	Baryonic feedback	18
3.5	Interacting Dark Energy models	19
3.5.1	Dark Scattering	21
4	Specific Objectives	24
5	Methodology and required techniques	25
5.1	Methodology	25
5.1.1	Simulations and dataset	25
5.2	ReACT	26
5.2.1	ReACT with neutrinos + baryons	27
5.3	CosmoPower	27
5.4	Cobaya	28
6	Progress	32
6.1	Implementation of the DS in ReACT	32
6.2	Validation of DS modelling	34
6.3	Including baryons and neutrinos	36
6.4	First publication	38
6.5	Creating a fast DS emulator	38
6.6	Adapting Cobaya to emulators	39
7	Workplan	42
	Bibliography	42

List of Figures

3.1	Energy density budget of the Universe	5
3.2	Halo model illustration	14
3.3	Reaction behaviour	17
3.4	Behavior of the DS interaction term	22
5.1	ReACT flowchart	26
5.2	Variation of T_{AGN}	27
5.3	Neuronal Network implemented in <code>CosmoPower</code>	28
6.1	w CDM+DS in ReACT vs simulations	34
6.2	CPL+DS in ReACT vs simulations	35
6.3	Degeneracy of neutrinos	36
6.4	Degeneracy of baryons	37
6.5	Dark Scattering emulation accuracy	39
6.6	CMB C_ℓ emulator in Cobaya	40
6.7	Linear $\mathcal{P}_L(k)$ emulator in Cobaya	41

Units

Throughout this document I will employ natural units, where the speed of light, the Planck constant and the Boltzmann constant are set to unity, i.e.

$$c \equiv \hbar \equiv k_B \equiv 1.$$

Notation

I have denoted "**dot**" and "**prime**" as derivatives respect to dynamical time t , and conformal time η , respectively.

I also have denoted the background of whichever quantity A with a bar \bar{A} .

Convention

Latin subscripts label i : 3D euclidean space \mathbb{R}^3 .

Greek subscripts label μ : 4D space-time \mathcal{M}^4 .

Our signs convention of the metric will be $(-, +, +, +)$.

Conversions

Electronvolt	1 GeV	=	1.602×10^{-19} J
Parsecs	1 pc	=	3.085×10^{16} m
Solar Mass	1 M_{\odot}	=	1.989×10^{30} kg
Barn	1 b	=	10^{-28} m ²

Table 1: Several useful conversions

Acronyms: **GR** (General Relativity), **FLRW** (Friedmann-Lemaître-Robertson-Walker), **CDM** (Cold Dark Matter), **DE** (Dark Energy), **LSS** (Large-Scale Structure), **IDE** (Interacting Dark Energy), **DS** (Dark Scattering), **FT** (Fourier Transform), **NN** (Neuronal Network).

MAIN GOAL

In the present project we aim to construct non-linear spectra and validate it through N-body simulations of structure formation within the Dark Scattering Dark Energy (DS) model. Moreover we shall include baryonic and neutrino effects in order to compute realistic spectra which we then contrast with simulated and real data. Such comparison will be performed through Bayesian parameter estimation of the elements of this model employing a variety of observations of large scale structure (LSS). Such goal is tackled through novel techniques to generate non-linear solutions to the matter fluctuations with the aid of the spherical collapse model, in order to predict halo spectra in dark energy theories. All this is contained in an implementation of the DS model within the ReACT code.

In a second stage of the project we produce thousands of non-linear matter Power Spectra through an emulator software in order to speed up the Bayesian analysis of data, comprising large optical galaxy catalogues and weak lensing data.

In a final stage of the project, we aim to program an emulator for spectra from 21cm intensity maps, and incorporate simulated sets of data from future surveys to complement the likelihood and model selection analyses of the DS dark energy model.

INTRODUCTION

In the near future cosmologist will benefit from the new generation of galaxy surveys, able to map large-scale structures (LSS) and lensing distortions out to high redshifts. Specifically, the stage IV surveys will be much bigger and deeper than their predecessors and will observe hundreds of millions of galaxies over a large fraction of the sky in the optical and radio wavelengths. Thereby, scientists will be able to probe much larger scales – approaching the size of the Hubble horizon, and determine the properties of the Universe with unprecedented precision. In particular, the aim is to elucidate the nature of the enigmatic dark sector components.

The current data is surprisingly compatible with the minimal and simplistic model called Λ CDM (Λ a cosmological constant + cold dark matter), but requires the existence of two exotic constituents; namely, dark energy – the mysterious substance that is ripping the Universe apart, and dark matter – the unobserved component that allowed the formation and keeps the stability of structures in the Universe. For our purposes, we shall focus on the former, which currently dominates the energy density budget of the Universe.

The established Λ CDM model is, however, under continuous scrutiny, due to tension of the H_0 value measured (see [Riess, 2019] a short review), which seems to depend on whether the observable signatures are based on the early or late Universe. Additionally, there is also a tension on the amplitude of density fluctuations encoded in the σ_8 (see [Douspis et al., 2018]) extrapolated to today. The state-of-the-art clustering and lensing measurements carried out by stage IV LSS surveys will tell us whether the late Universe’s accelerated expansion is due to a simple cosmological constant, an evolving scalar field, or a modification of gravity. In the present project, I am interested in studying the interacting models of the dark sector since they have shown to diminish such tensions (see [Di Valentino et al., 2020], [Yao & Meng, 2022], [Gao et al., 2021]).

Throughout the PhD program, I have been learning the theory behind simulating the cosmological signal and the observations for physically motivated models of interacting dark energy (IDE), in the spirit of [Bose et al., 2018]. Specifically, I will focus on an interaction consisting of pure momentum transfer with CDM, named Dark Scattering (DS) model (see [Baldi & Simpson, 2015], [Pourtsidou & Tram, 2016], [Pourtsidou et al., 2013]). In addition, this project involves comparing simulation products of large datasets against theoretical predictions through a modified halo model code. Moreover, I have gained hands-on experience of employing machine learning techniques to emulate our predictions in terms of the matter spectra, in order to perform very fast statistical tests by including emulators, specifically model selection and cosmological parameter estimation, with the aid of available galaxy data measured from recent surveys and galaxy synthetic data. During this stage, I have helped modifying codes in Python and C/C++, which involve high performance computing using dedicated facilities at UNAM and Edinburgh. I will also aim to get involved in large collaborations, where Dr. Alkistis Pourtsidou holds leadership positions.

At this point, as a last objective I will use the acquired experience to provide emulators for modelling the 21cm signal, expected to be detected in the near future by the forthcoming radio telescopes.

This document is organized as follows: In chapter 3 I describe the theoretical elements of the project, such as, cosmological perturbation theory, IDE theory and halo model reaction. Following in chapter 4, I highlight out the specific objectives for this project. In chapter 5 I will focus on the

methods and codes that will be employed to compute the theoretical spectra numerically, and to perform statistical tests. Subsequently, in chapter 6, I will report my current progress and lastly in chapter 7, I propose the workplan for the rest of this PhD project.

PRECEDENTS

Throughout this chapter, I will focus on describing in detail the state-of-art of cosmological tools that will be crucial for developing this PhD project.

3.1 Background cosmology

Cosmology has been evolving throughout the decades in light of new observations provided by technological advances in telescopes and space satellites, for example, from observations of the CMB by **COBE** (1989) and **WMAP** (2001) missions to the more recent **Planck** (2009) satellite. Likewise, galaxy surveys responsible for mapping the Large-Scale Structure (LSS) like **SDSS** (2000) and **DES** (2013) continue evolving, with experiments that start operation in the coming years, such as **DESI**, **Euclid**, **LSST**, and **SKA** and its precursor **MeerKAT**. A wealth of precise measurements, together with a meticulous treatment of this new information, will adjust or extend predictions from our cosmological theories about the content, structure, origin and evolution of the Universe.

The main axiom of cosmology is the: *Cosmological Principle*, which states that "for scales sufficiently large (at least 100-150 Mpc) the distribution of the LSS ought to be statistically isotropic and homogeneous". Our picture of the CMB is the best proof of concordance with such principle. In cosmology we often resort to *General Relativity* (GR) framework to describe the space-time of the Universe, since GR is the most successful theory that explains gravity, from the Solar system scales to the size of the Hubble horizon. An exact solution to Einstein's equations meeting the conditions of the cosmological principle is the Friedmann-Lemaître-Robertson-Walker (FLRW) metric, with the line element as:

$$ds^2 = g_{\mu\nu}dx^\mu dx^\nu = -dt^2 + a^2(t) \left[\frac{d\chi^2}{1 - K\chi^2} + \chi^2 d\theta^2 + \chi^2 \sin^2\theta d\varphi^2 \right], \quad (3.1)$$

where $a(\eta)$ is the scale factor and K is the curvature of the space. Interestingly, an important feature of FLRW solution is the fact that a static Universe requires fine-tuning: the Universe must be on expanding or contracting depending on the kind of matter that conforms it, and therefore, the light from distant objects must be redshifted or blueshifted accordingly. So, assuming that each Universe component can be described as a perfect fluid with density as ρ and pressure as P , then, the energy-momentum tensor is given by,

$$T_{\mu\nu} = (\rho + P) u_\mu u_\nu + P g_{\mu\nu}. \quad (3.2)$$

The cosmological principle forces the macroscopic velocity to be isotropic, i.e. the 4-velocity of a comoving observer only has one temporal component, $u^\mu = (1, 0, 0, 0)$. Thus, the evolution equations of the metric dictated from Einstein's field equations with a cosmological constant are:

$$H^2 = \left(\frac{\dot{a}}{a} \right)^2 = \frac{8\pi G}{3} \rho + \frac{\Lambda}{3} - \frac{K}{a^2}. \quad \text{Friedmann Equation,} \quad (3.3)$$

with H the rate of expansion or often called as *Hubble parameter*. Additionally, the trace of Einstein's field equations yields

$$\frac{\ddot{a}}{a} = -\frac{4\pi G}{3} \left(\rho + \frac{3P}{c^2} \right) + \frac{\Lambda}{3}. \quad \text{Raychaudhuri Equation.} \quad (3.4)$$

In order to close the system it is necessary to specify the matter content, so that the number of degrees of freedom matches the number of equations. This is commonly done by specifying an equation of state with a parameter as: $P = w\rho$.

The solutions of such equations provide a variety of universes that would be governed by several ingredients, such as; baryons, cold dark matter (CDM), dark energy, photons, neutrinos, scalar fields, curvature and so on. Depending on their energy contributions, an universe that fits with our observations can be predicted, an analogy of this is like identifying a suspect with his/her fingerprint. Nowadays, we know that the majority of observations support extremely well that the Universe is mainly constituted by matter (mostly CDM + baryons), radiation and, in most part, by the enigmatic dark energy. Remarkably, the dark sector currently accounts for $\sim 95\%$ of the energy density budget of the Universe (see Figure 3.1). Then, our deepest understanding of the Universe is captured by a simple, elegant concept, the ultimate model of cosmology, is so-called Λ CDM. Alternatively, and aiming to better understand the dark energy, there are other approaches that extend the standard model by a parametrization of its equation of state. The simplest is a constant $w \neq -1$, a model which we name w CDM. Moreover, a Taylor expansion of the equation of state as a function of redshift yields the minimal expression $w(a) = w_0 + w_a(1 - a)$, well-known as Chevallier-Polarski-Linder (CPL) model [Chevallier & Polarski, 2001].

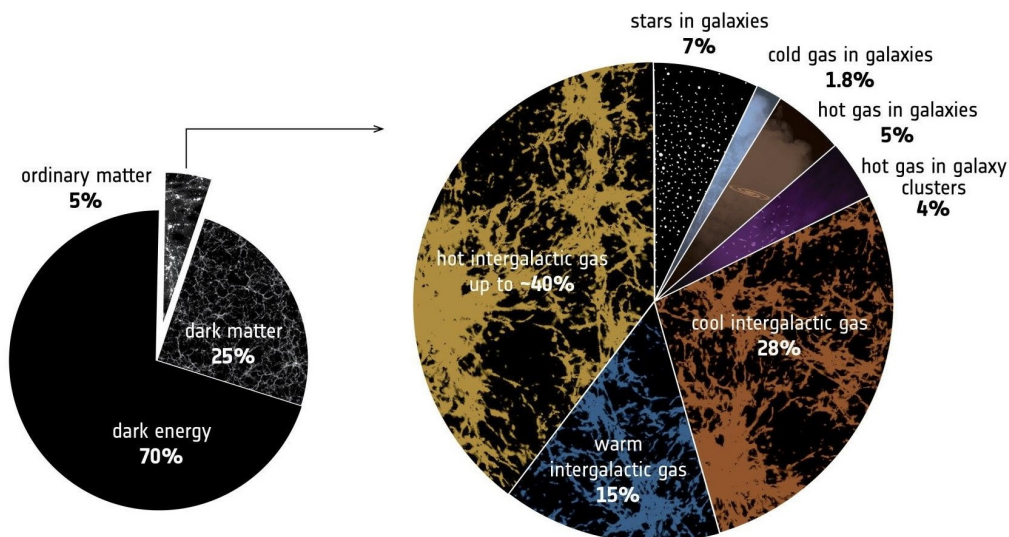


Figure 3.1: Pie chart of the cosmic energy budget today. The dark sector mostly dominates the Universe, whereas the baryonic density (mostly intergalactic gas) amounts to only about 5%. Image courtesy from ESA.

All these models do not come without caveats. Cosmologists are engaged in a tremendous discussion about constraining the today's Hubble constant value H_0 with values dissimilar from different observables (see [Di Valentino et al., 2021], [Verde et al., 2019]). This data tension on the H_0 value seems to depend on whether the measurements are based on the early Universe or more directly measured from the late Universe. The CMB data yields an estimation of $H_0 = 67.4 \pm 0.5 \text{ km s}^{-1}\text{Mpc}^{-1}$, whose best fit of Λ CDM parameters are combined to acquire the most precise H_0 estimation of all probes. Whereas the late Universe, for example the project of SHOES (Supernovae H0 for the Equation of State) yields an estimation of $H_0 = 73.5 \pm 1.4 \text{ km s}^{-1}\text{Mpc}^{-1}$, which is in 4.2σ tension with the early Universe estimation! It is likely that our current lack of understanding about the nature dark energy and dark matter

might be causing this discrepancy, thus giving room to more alternative models of dark sector that have been extensively proposed in the literature (e.g modified gravity, $f(R)$ models, quintessence field, scalar field dark matter, Hordenski models, among others). In addition, since in Λ CDM the dark sector is considered uncoupled is just an ad-hoc assumption of the model, there is another interesting approach, which are the models we will focus on for this project, called interacting dark energy (IDE).

3.2 Cosmological Perturbation Theory

We have discussed a statistically homogeneous and isotropic universe, valid only on large scales. However, this description is not even close to the Universe we live in. The perturbative treatment has been a powerful tool in physics, while in Cosmology is very accurate in predicting the evolution of inhomogeneities at some stages. In Cosmological Perturbation Theory (CPT) ([Bernardeau et al., 2002], [Ellis et al., 2012], [Dodelson & Schmidt, 2020]) approaches the background spacetime is mostly assumed to be the flat FLRW Universe while the perturbed spacetime is curved, with the corresponding matter perturbations. Nonetheless, the Newtonian limit is appropriate describing scales smaller than Hubble horizon (i.e. smaller than super-horizon scales) and also for non-relativistic matter components. For a rigorous description one must resort to perturbations in the framework of GR ([Malik & Wands, 2009]).

In this section we followed the same notation from [Bernardeau et al., 2002] in order to obtain the non-linear perturbations¹. The central idea in a perturbed analysis; is to slightly modify each quantity by a small linear quantity, i.e., $\mathcal{Y}(\mathbf{x}, \eta) \equiv \bar{\mathcal{Y}} + \delta\mathcal{Y}$, where \mathcal{Y} can be ρ , P , \mathbf{v} , or ϕ . Here we introduce several important quantities like **the density contrast** as $\delta(\mathbf{x}, \eta) \equiv \delta\rho/\bar{\rho}$, the peculiar velocity flow $\delta\mathbf{v} \equiv \mathbf{u}(\mathbf{x}, \eta) = d\mathbf{x}/d\eta$ and $\delta\phi \equiv \Phi(\mathbf{x}, \eta)$ the cosmological gravitational potential which is subject to the Poisson equation (on the Newtonian limit to GR):

$$\nabla_{\mathbf{x}}^2\Phi(\mathbf{x}, \eta) = \frac{3}{2}\Omega_m\mathcal{H}^2\delta(\mathbf{x}, \eta). \quad (3.5)$$

The Lagrangian for a single particle in a gravitational potential ϕ is

$$L = \frac{1}{2}m\dot{\mathbf{r}}^2 - m\phi, \quad (3.6)$$

which implies an equation of motion given by,

$$\dot{\mathbf{u}} = -H\mathbf{u} - \nabla_{\mathbf{r}}\Phi \quad \text{or} \quad \frac{\partial\mathbf{p}}{\partial\eta} = -ma\nabla_{\mathbf{x}}\Phi, \quad (3.7)$$

being $\mathbf{p} = ma\mathbf{u}$.

Vlasov equation.- In physics the Vlasov equation is used to describe dissipative systems of interactive particles by defining the particle number density in the phase-space $f(\mathbf{x}, \mathbf{p}, \eta)$. Vlasov described an infinite chain of self-linking equations for the distribution functions of random variables (see [Perepelkin et al., 2018]). Thus, the phase-space conservation implies,

$$\frac{df}{d\eta} = \frac{\partial f}{\partial\eta} + \frac{\partial f}{\partial\mathbf{x}} \cdot \frac{\partial\mathbf{x}}{\partial\eta} + \frac{\partial f}{\partial\mathbf{p}} \cdot \frac{\partial\mathbf{p}}{\partial\eta} = 0. \quad (3.8)$$

¹Hereafter we are going to take advantage of the comoving coordinates: $\mathbf{r} = a(t)\mathbf{x}$, where \mathbf{x} is referred to as the comoving distance, \mathbf{r} is simply the physical distance. Similarly, making use of the conformal time η which is related to the cosmic time t by integrating $d\eta = dt/a(t)$. In addition, allows us to express the conformal Hubble parameter as $\mathcal{H} = aH$.

This is called the **Vlasov equation**. In terms of (3.7), we obtain,

$$\frac{df}{d\eta} = \frac{\partial f}{\partial \eta} + \frac{\mathbf{p}}{ma} \cdot \frac{\partial f}{\partial \mathbf{x}} - ma \nabla_{\mathbf{x}} \Phi \cdot \frac{\partial f}{\partial \mathbf{p}} = 0. \quad (3.9)$$

The zeroth-order moment relates the phase-space density to the conformal density field through the next equation,

$$\int d^3\mathbf{p} f(\mathbf{x}, \mathbf{p}, \eta) \equiv \rho(\mathbf{x}, \eta). \quad (3.10)$$

The first moment is related to the velocity field of particles,

$$\int d^3\mathbf{p} \frac{\mathbf{p}}{ma} f(\mathbf{x}, \mathbf{p}, \eta) \equiv \rho(\mathbf{x}, \eta) \mathbf{u}(\mathbf{x}, \eta). \quad (3.11)$$

Finally, in order to derive the Euler equation we only integrate upto the second moment,

$$\int d^3\mathbf{p} \frac{p_i p_j}{m^2 a^2} f(\mathbf{x}, \mathbf{p}, \eta) \equiv \rho(\mathbf{x}, \eta) u_i u_j + \sigma_{ij}. \quad (3.12)$$

The term σ_{ij} encodes generalized pressure forces, therefore, in the absence of any pressure perturbation (which is our case for cold pressure-less matter) we obtain $\sigma_{ij} = 0$ (see [Dodelson & Schmidt, 2020]).

The continuity equation is derived by just \mathbf{p} -integrating Eq. (3.9) and applying the definition of moments (3.10) and (3.11). Thus, in terms of $\delta(\mathbf{x}, \eta)$:

$$\frac{\partial \delta}{\partial \eta} + \nabla_{\mathbf{x}} \cdot [(1 + \delta) \mathbf{u}] = 0. \quad (3.13)$$

Subsequently, the Euler equations are derived by considering the first moment² of (3.9) and reducing terms to obtain the following,

$$\frac{\partial \mathbf{u}}{\partial \eta} + (\mathbf{u} \cdot \nabla_{\mathbf{x}}) \mathbf{u} + \mathcal{H} \mathbf{u} + \nabla_{\mathbf{x}} \Phi = 0. \quad (3.14)$$

Applying the divergence and substituting the Poisson equation (3.5),

$$\frac{\partial \theta}{\partial \eta} + \nabla_{\mathbf{x}} \cdot (\mathbf{u} \cdot \nabla_{\mathbf{x}}) \mathbf{u} + \mathcal{H} \theta + \frac{3}{2} \Omega_m \mathcal{H}^2 \delta = 0, \quad (3.15)$$

where we have introduced the velocity divergence $\theta \equiv \nabla_{\mathbf{x}} \cdot \mathbf{u}$ which is common named as **the volume expansion rate** (the 3D version of H). Note that on the Euler equation the curl contribution of the velocity $\omega \equiv \nabla_{\mathbf{x}} \times \mathbf{u}$, or the vorticity, has not been included, because the vorticity decays ($\omega \propto 1/a$) with the expansion, then it can safely be neglected at late times.

3.2.1 Linear regime

The non-linear equations (3.13) and (3.14), can be linearized by removing the higher orders. The continuity equation yields,

$$\frac{\partial \delta}{\partial \eta} + \theta = 0, \quad (3.16)$$

Moreover, we reduce the Euler equation (3.15) at linear order, and working in Fourier space, where at linear order the k -modes evolve independently, we have

²Bear in mind that the distribution function f evaluated at the boundary vanishes, since f does not include particles with infinite momentum.

$$\frac{\partial \mathbf{u}}{\partial \eta} + \mathcal{H} \mathbf{u} + \nabla_{\mathbf{x}} \Phi = 0, \quad \Rightarrow \quad \frac{\partial \tilde{\theta}_{\mathbf{k}}}{\partial \eta} + \mathcal{H} \tilde{\theta}_{\mathbf{k}} - k^2 \Phi = 0 \quad (3.17)$$

Combing Eqs. (3.5) and (3.16) on Eq. (3.17), we arrive at an equation purely for the density contrast:

$$\frac{\partial^2 \tilde{\delta}_{\mathbf{k}}(\eta)}{\partial \eta^2} + \mathcal{H} \frac{\partial \tilde{\delta}_{\mathbf{k}}(\eta)}{\partial \eta} - \frac{3}{2} \Omega_m \mathcal{H}^2 \tilde{\delta}_{\mathbf{k}}(\eta) = 0. \quad (3.18)$$

The two solutions of (3.18) could be expressed as

$$\tilde{\delta}_{\mathbf{k}}(\eta) = D_+(\eta) A_{\mathbf{k}} + D_-(\eta) B_{\mathbf{k}}. \quad (3.19)$$

where D_{\pm} is the **linear growth factor** and decay factor respectively, and they depend purely on the background quantities. Assuming a period of primordial inflation, the decay mode would vanish due to the accelerating expansion. Thus, we will not consider it. As a result of solution (3.19), we also solve for θ by using (3.16) and using $d/d \ln D_+ = (\mathcal{H}f)^{-1} d/d\eta$,

$$\tilde{\theta}_{\mathbf{k}}(\eta) = -\mathcal{H}(\eta) f A_{\mathbf{k}}, \quad (3.20)$$

where, we have defined one relevant quantity

$$f = \frac{d \ln D_+}{d \ln a}. \quad (3.21)$$

The so-called **growth rate function** f . For example, considering on (3.18) an Einstein-de Sitter (EdS) universe where $\Omega_m = 1$ and $\Omega_{\Lambda} = 0$. Then, we would obtain the solution $\tilde{\delta}_{\mathbf{k}}^{\text{EdS}}(\mathbf{x}, \eta) = A_{\mathbf{k}} a(\eta)$, consequently $f = 1$. So, the growth factor scales as $a(\eta)$, with the normalization $D_+(a_0) = 1$. This result is very useful for describing an overdensity through a top-hat model, as described later.

3.2.2 Non-linear regime

Presently the linear order is accurate on large scales because the contrast density is in order of $\delta \ll 1$. However, from their initial size $\delta \approx 10^{-5}$ these perturbations will be growing on subhorizon scales and the scheme will be thoroughly different, the linear regime is no longer valid once δ approaches to one. Our task now is to extend CPT to the non-linear regime. So, we start moving to the right-hand the non-linear terms to express the equations as,

$$\delta' + \theta = -\delta \theta - (\mathbf{u} \cdot \nabla_{\mathbf{x}} \delta). \quad (3.22)$$

$$\theta' + \mathcal{H} \theta + \frac{3}{2} \Omega_m \mathcal{H}^2 \delta = -(\mathbf{u} \cdot \nabla_{\mathbf{x}}) \theta - [\nabla_{\mathbf{x}} (\mathbf{u} \cdot \nabla_{\mathbf{x}}) \cdot \mathbf{u}]. \quad (3.23)$$

As we did before, it is useful to describe the matter fields by resorting to Fourier space. The convention of the Fourier Transform (FT) applied to any given field Θ is,

$$\tilde{\Theta}(\mathbf{k}, \eta) = \int d^3 x \exp(-i \mathbf{k} \cdot \mathbf{x}) \Theta(\mathbf{x}, \eta), \quad \text{and} \quad \Theta(\mathbf{x}, \eta) = \int \frac{d^3 k}{(2\pi)^3} \exp(i \mathbf{k} \cdot \mathbf{x}) \tilde{\Theta}(\mathbf{k}, \eta). \quad (3.24)$$

To extend the solutions beyond the linear order, fields will be expressed as infinite perturbative series, by setting them in configuration space and Fourier space as follows,

$$\Theta(\mathbf{x}, \eta) = \sum_{n=1}^{\infty} \Theta^{(n)}(\mathbf{x}, \eta), \quad \Rightarrow \quad \tilde{\Theta}(\mathbf{k}, \eta) = \sum_{n=1}^{\infty} \tilde{\Theta}^{(n)}(\mathbf{k}, \eta). \quad (3.25)$$

The subscript (n) establishes the perturbative order, e.g. the density field case $\delta^{(1)}$ and $\theta^{(1)}$ represents the fields at linear order. As stated earlier, at very late times, the linear order can be rewritten as

$$\delta^{(1)}(\mathbf{x}, \eta) = \delta_0(\mathbf{x})D_+(\eta) \quad (3.26)$$

Normalized at the present time η_0 , such that, $\delta_0(\mathbf{x}) = \delta(\mathbf{x}, \eta_0)$ and the velocity field is given by Eq. (3.20). We will follow the standard approach (see [Dodelson & Schmidt, 2020]) to solve the non-linearities. From the non-linear terms of equations (3.22) and (3.23).

$$\sum_{n=1}^{\infty} \delta'^{(n)} + \sum_{n=1}^{\infty} \theta^{(n)} = - \sum_{n=1}^{\infty} \sum_{k=1}^{\infty} \delta'^{(n)} \theta^{(k)} - \sum_{n=1}^{\infty} \sum_{k=1}^{\infty} (\mathbf{u}^{(n)} \cdot \nabla_{\mathbf{x}} \delta^{(k)}) . \quad (3.27)$$

$$\begin{aligned} \sum_{n=1}^{\infty} \theta'^{(n)} + \mathcal{H} \sum_{n=1}^{\infty} \theta^{(n)} + \frac{3}{2} \Omega_m \mathcal{H}^2 \sum_{n=1}^{\infty} \delta^{(n)} = & - \sum_{n=1}^{\infty} \sum_{k=1}^{\infty} (\mathbf{u}^{(n)} \cdot \nabla_{\mathbf{x}}) \theta^{(k)} \\ & - \sum_{n=1}^{\infty} \sum_{k=1}^{\infty} [\nabla_{\mathbf{x}}(\mathbf{u}^{(n)} \cdot \nabla_{\mathbf{x}}) \cdot \mathbf{u}^{(k)}] . \end{aligned} \quad (3.28)$$

Following the perturbative order hierarchy, each term of the equation is going to be truncated depending on the order imposed, as follows:

$$\text{1st order:} \quad \delta'^{(1)} + \theta^{(1)} = 0. \quad (3.29)$$

$$\theta'^{(1)} + \mathcal{H}\theta^{(1)} + \frac{3}{2} \Omega_m \mathcal{H}^2 \delta^{(1)} = 0. \quad (3.30)$$

$$\text{2nd order:} \quad \delta'^{(2)} + \theta^{(2)} = - \delta^{(1)} \theta^{(1)} - \mathbf{u}^{(1)} \cdot \nabla_{\mathbf{x}} \delta^{(1)}. \quad (3.31)$$

$$\theta'^{(2)} + \mathcal{H}\theta^{(2)} + \frac{3}{2} \Omega_m \mathcal{H}^2 \delta^{(2)} = - (\mathbf{u}^{(1)} \cdot \nabla_{\mathbf{x}}) \theta^{(1)} - [\nabla_{\mathbf{x}}(\mathbf{u}^{(1)} \cdot \nabla_{\mathbf{x}}) \cdot \mathbf{u}^{(1)}] . \quad (3.32)$$

$$\text{3rd order:} \quad \delta'^{(3)} + \theta^{(3)} = - \delta^{(2)} \theta^{(1)} - \delta^{(1)} \theta^{(2)} - \mathbf{u}^{(2)} \cdot \nabla_{\mathbf{x}} \delta^{(1)} - \mathbf{u}^{(1)} \cdot \nabla_{\mathbf{x}} \delta^{(2)}. \quad (3.33)$$

$$\begin{aligned} \theta'^{(3)} + \mathcal{H}\theta^{(3)} + \frac{3}{2} \Omega_m \mathcal{H}^2 \delta^{(3)} = & - (\mathbf{u}^{(2)} \cdot \nabla_{\mathbf{x}}) \theta^{(1)} - (\mathbf{u}^{(1)} \cdot \nabla_{\mathbf{x}}) \theta^{(2)} - [\nabla_{\mathbf{x}}(\mathbf{u}^{(2)} \cdot \nabla_{\mathbf{x}}) \cdot \mathbf{u}^{(1)}] \\ & - [\nabla_{\mathbf{x}}(\mathbf{u}^{(1)} \cdot \nabla_{\mathbf{x}}) \cdot \mathbf{u}^{(2)}] . \end{aligned} \quad (3.34)$$

⋮

Note that the Poisson equation holds at each order, because it is a linear relation between fields. Then, we can write³ yields

$$\nabla_{\mathbf{x}}^2 \Phi^{(n)}(\mathbf{x}, \eta) = \frac{3}{2} \Omega_m \mathcal{H}^2 \delta^{(n)}(\mathbf{x}, \eta), \quad \Rightarrow \quad \tilde{\Phi}^{(n)}(\mathbf{k}, \eta) = -\frac{3}{2} \Omega_m \frac{\mathcal{H}^2}{k^2} \tilde{\delta}^{(n)}(\mathbf{k}, \eta). \quad (3.35)$$

For illustrative purposes, we explore only at 2nd order. So, working in Fourier space on Eqs. (3.31) and (3.32), where we have applied the convolution theorem and Dirac delta δ_D properties, one obtains,

³Similarly, the peculiar velocity at 1st order would be given by: $\tilde{u}^{(1)}(\mathbf{k}, \eta) = i \frac{\mathbf{k}}{k^2} \mathcal{H} f(\eta) \tilde{\delta}^{(1)}(\mathbf{k}, \eta)$.

$$\begin{aligned} \tilde{\delta}^{(2)}(\mathbf{k}, \eta) + \tilde{\theta}^{(2)}(\mathbf{k}, \eta) &= \int \frac{d^3 k_1}{(2\pi)^3} \int d^3 k_2 \delta_D(\mathbf{k} - \mathbf{k}_1 - \mathbf{k}_2) \left[1 + \frac{(\mathbf{k}_1 \cdot \mathbf{k}_2)}{k_1^2} \right] \\ &\times \left[\mathcal{H}f(\eta) \tilde{\delta}^{(1)}(\mathbf{k}_1, \eta) \tilde{\delta}^{(1)}(\mathbf{k}_2, \eta) \right], \end{aligned} \quad (3.36)$$

$$\begin{aligned} \tilde{\theta}^{(2)} + \mathcal{H}\tilde{\theta}^{(2)} + \frac{3}{2}\Omega_m \mathcal{H}^2 \tilde{\delta}^{(2)} &= \int \frac{d^3 k_1}{(2\pi)^3} \int d^3 k_2 \delta_D(\mathbf{k} - \mathbf{k}_1 - \mathbf{k}_2) \left[\frac{(\mathbf{k}_1 \cdot \mathbf{k}_2)}{k_1^2} + \frac{(\mathbf{k}_1 \cdot \mathbf{k}_2)^2}{k_1^2 k_2^2} \right] \\ &\times \left[(\mathcal{H}f(\eta))^2 \tilde{\delta}^{(1)}(\mathbf{k}_1, \eta) \tilde{\delta}^{(1)}(\mathbf{k}_2, \eta) \right]. \end{aligned} \quad (3.37)$$

Rewriting the derivatives as $\partial/\partial \ln D_+ = (\mathcal{H}f)^{-1} \partial/\partial \eta$ and rescaling the velocity field like $\tilde{\vartheta}^{(2)} \equiv \tilde{\theta}^{(2)}/(\mathcal{H}f)$, in order to simplify equations, we have,

$$\frac{\partial \tilde{\delta}^{(2)}(\mathbf{k}, D_+)}{\partial \ln D_+} + \tilde{\vartheta}^{(2)}(\mathbf{k}, D_+) = D_+^2 I_1(\mathbf{k}), \quad (3.38)$$

$$\frac{\partial \tilde{\vartheta}^{(2)}(\mathbf{k}, D_+)}{\partial \ln D_+} + \left[\frac{3}{2} \frac{\Omega_m}{f^2} - 1 \right] \tilde{\vartheta}^{(2)}(\mathbf{k}, D_+) + \frac{3}{2} \frac{\Omega_m}{f^2} \tilde{\delta}^{(2)}(\mathbf{k}, D_+) = D_+^2 I_2(\mathbf{k}). \quad (3.39)$$

where I_1 and I_2 are the non-linear integrals respectively that only depend on \mathbf{k} . In general for dark energy cosmologies with similar expansion histories, it turns out that the quantity $\Omega_m(\eta)/f^2(\eta)$ is very close to 1 throughout time. Thus, the only terms in Eqs. (3.38) and (3.39) that depend explicitly on time (via D_+) are the source terms. This leads us to make the following power-law ansatz:

$$\tilde{\delta}^{(2)} = C_1(\mathbf{k}) D_+^m, \quad \text{and} \quad \tilde{\vartheta}^{(2)} = C_2(\mathbf{k}) D_+^m. \quad (3.40)$$

Then,

$$mC_1 D_+^m + C_2 D_+^m = D_+^2 I_1(\mathbf{k}), \quad (3.41)$$

$$mC_2 D_+^m + \frac{1}{2} C_2 D_+^m + \frac{3}{2} C_1 D_+^m = D_+^2 I_2(\mathbf{k}). \quad (3.42)$$

Clearly, the only solution is given by the case $m = 2$ and,

$$C_1 = + \frac{5}{7} I_1(\mathbf{k}) - \frac{2}{7} I_2(\mathbf{k}), \quad (3.43)$$

$$C_2 = - \frac{3}{7} I_1(\mathbf{k}) + \frac{4}{7} I_2(\mathbf{k}). \quad (3.44)$$

Finally, we can write the solutions at second order in terms of η ,

$$\tilde{\delta}^{(2)}(\mathbf{k}, \eta) = D_+^2 \int \frac{d^3 k_1}{(2\pi)^3} \int d^3 k_2 \delta_D(\mathbf{k} - \mathbf{k}_1 - \mathbf{k}_2) F_2(\mathbf{k}_1, \mathbf{k}_2) \delta_0(\mathbf{k}_1) \delta_0(\mathbf{k}_2), \quad (3.45)$$

$$\tilde{\vartheta}^{(2)}(\mathbf{k}, \eta) = - D_+^2 \int \frac{d^3 k_1}{(2\pi)^3} \int d^3 k_2 \delta_D(\mathbf{k} - \mathbf{k}_1 - \mathbf{k}_2) G_2(\mathbf{k}_1, \mathbf{k}_2) \delta_0(\mathbf{k}_1) \delta_0(\mathbf{k}_2). \quad (3.46)$$

where F_2 and G_2 are the symmetrized kernels at second order,

$$F_2(\mathbf{k}_1, \mathbf{k}_2) = \frac{5}{7} + \frac{2}{7} \frac{(\mathbf{k}_1 \cdot \mathbf{k}_2)^2}{k_1^2 k_2^2} + \frac{1}{2} (\mathbf{k}_1 \cdot \mathbf{k}_2) \left(\frac{k_1}{k_2} + \frac{k_2}{k_1} \right), \quad (3.47)$$

$$G_2(\mathbf{k}_1, \mathbf{k}_2) = \frac{3}{7} + \frac{4}{7} \frac{(\mathbf{k}_1 \cdot \mathbf{k}_2)^2}{k_1^2 k_2^2} + \frac{1}{2} (\mathbf{k}_1 \cdot \mathbf{k}_2) \left(\frac{k_1}{k_2} + \frac{k_2}{k_1} \right). \quad (3.48)$$

This approach is extended to higher orders, and the n -th order solution would be written as,

$$\tilde{\delta}^{(n)}(\mathbf{k}, \eta) = D_+^n \left[\prod_{i=1}^n \int \frac{d^3 k_i}{(2\pi)^3} \right] (2\pi)^3 \delta_D \left(\mathbf{k} - \sum_{i=1}^n \mathbf{k}_i \right) F_n(\mathbf{k}_1, \dots, \mathbf{k}_n) \delta_0(\mathbf{k}_1) \cdots \delta_0(\mathbf{k}_n), \quad (3.49)$$

$$\tilde{\vartheta}^{(n)}(\mathbf{k}, \eta) = -D_+^n \left[\prod_{i=1}^n \int \frac{d^3 k_i}{(2\pi)^3} \right] (2\pi)^3 \delta_D \left(\mathbf{k} - \sum_{i=1}^n \mathbf{k}_i \right) G_n(\mathbf{k}_1, \dots, \mathbf{k}_n) \delta_0(\mathbf{k}_1) \cdots \delta_0(\mathbf{k}_n). \quad (3.50)$$

Certainly $F_1 = 1$ and $G_1 = 1$. A strategy to determine the kernels F_n and G_n is by resorting to recurrence formulae or solve them numerically. This result allows us to explicitly calculate how structure in the universe evolves nonlinearly. This however, is limited to only dark matter, and does not take into account shell crossing stages, halo formation, or baryonic effects (galaxy), among others.

3.2.3 Power spectrum

The most important aspect of CPT is that allows us to connect the evolved perturbations to statistics of quantities that are deemed **cosmological observables**. We will focus on describing the statistics of the linear field $\delta_0(\mathbf{r})$ (here subscripted by 0) in order to yield the **Matter Power spectrum** $\mathcal{P}(\mathbf{k})$. A good starting point is thinking about the probability of find one particle, galaxy or halo within a volume dV_1 , as $P_1 = \bar{n} dV_1$, where $\bar{n} = \langle \rho \rangle$ is the mean density. Whereas, the probability of finding another one in dV_2 , separated by a distance \mathbf{r} would be written as:

$$P_2(\mathbf{r}) = \bar{n} [1 + \xi(\mathbf{r})] dV_1 dV_2. \quad (3.51)$$

The probability excess $\xi(\mathbf{r})$ is well-known as the two-point correlation function (2PCF). Furthermore, under Inflation prediction, the distribution of the primordial density fluctuations are Gaussian is directly inherited up to the matter fields. This allows us to describe $\delta(\mathbf{r})$ as **Gaussian fields** that were produced by some random process in the early universe. Then, the 2PCF⁴ can be defined in terms of the density contrast⁵,

$$\xi(\mathbf{r}) \equiv \langle \delta_0(\mathbf{r}') \delta_0(\mathbf{r}' + \mathbf{r}) \rangle. \quad (3.52)$$

There are several theoretical models to estimate the 2PCF via comparing it to a random sample (see [Kerscher et al., 2000]). Now, we can set the 2PCF in Fourier representation in order to define the matter power spectrum $\mathcal{P}(\mathbf{k})$,

$$\mathcal{P}_L(\mathbf{k}) \equiv \int d^3 \mathbf{r} \xi(\mathbf{r}) \exp(-i\mathbf{k} \cdot \mathbf{r}). \quad (3.53)$$

⁴A clear disadvantage of the 2PCF is that it does not show the full description for non-Gaussian fields. In such case one must resort to higher-order statistics (for example a candidate for the statistical estimator beyond 2PCF is the 3PCF).

⁵Notice, $\langle \cdot \rangle$ denotes an ensemble average. For instance, means the average overdensity at for many realizations of the random process.

Finally, also due to isotropy symmetry (rotation invariance) $\mathcal{P}_L(\mathbf{k}) = \mathcal{P}_L(k)$ and considering homogeneity (translation invariance) the power spectra is usually expressed as,

$$\langle \delta_0(\mathbf{k})\delta_0(\mathbf{k}') \rangle = (2\pi)^3 \delta_D(\mathbf{k} + \mathbf{k}') \mathcal{P}_L(k). \quad (3.54)$$

As result of Inflation theory, the initial condition of the power spectrum is predicted in a power-law form like,

$$\mathcal{P}(k) = A_s \left(\frac{k}{k_*} \right)^{n_s-1} \cdot T^2(k), \quad (3.55)$$

where A_s is the primordial scalar amplitude, $k_* = 0.05$ Mpc is the pivot scale guarantees homogeneity and isotropy, n_s represents the spectral index and $T^2(k)$ is the transfer function that contains messy physics of evolution of density perturbations. Conventionally, a dimensionless power spectra is often more useful, given by,

$$\Delta(k) = \frac{k^3 \mathcal{P}(k)}{2\pi^2}. \quad (3.56)$$

Regarding its the statistical meaning, from Eq (3.54) we deduce the power spectrum is an approach to estimate the variance of density distribution, since the mean of δ_0 must be zero. Thus, we can calculate the variance $\sigma^2(R)$ for a smoothed density field as follows,

$$\sigma^2(R) = \int d \ln k |W(kR)|^2 \Delta(k). \quad (3.57)$$

Popular choice of the smoothing window function $W(rR)$ is a top-hat filter in real space, then in Fourier space is $W(kR) = 3j_1(kR)/kR$ with a characteristic smoothing scale $R = (3M/4\pi\rho)^{\frac{1}{3}}$. So, indeed! We can generate observables from cosmological perturbations as we just illustrated on the matter power spectrum. Another interesting observable is named σ_8 and is basically evaluating the (3.57) at $R = 8$ Mpc,

$$\sigma_8 \equiv \sigma(R = 8 \text{ Mpc}, z = 0). \quad (3.58)$$

This quantity is also fairly relevant nowadays, on giving information about structure formation. However, unfortunately this quantity carries a data tension as well. Particularly on both parameters (Ω_m, σ_8) or more often find in literature as $S_8 \equiv \sigma_8 \sqrt{\Omega_m/0.3}$. From Planck 2018 CMB measurements ([Aghanim et al., 2020]) is estimated to be $S_8 = 0.825 \pm 0.011$, whereas DES collaboration ([Abbott et al., 2022]) derives an estimation of $S_8 = 0.776 \pm 0.017$ and KiDS-1000 (see [Heymans et al., 2021]) reports a value of $S_8 = 0.766^{+0.020}_{-0.014}$ for low-redshift, thus, discrepancies are around $2 - 2.5\sigma$ respect to Planck. Although such discrepancies could be belonged from systematic causes that cannot entirely be ruled out.

Regarding of obtaining an accurate prediction on the matter distribution, we further extend our analysis by inserting all correlations of the non-linear matter field $\delta(\mathbf{x}, \eta)$ to construct the non-linear correction on the matter power spectrum, like

$$\langle \delta(k, \eta)\delta(k', \eta) \rangle = \sum_n \sum_m \langle \delta^{(n)}(k, \eta)\delta^{(m)}(k', \eta) \rangle. \quad (3.59)$$

Making use of the Wick's theorem, and the fact that δ is assumed to be Gaussian, thus, if $n + m = \text{odd}$, the contribution is zero, otherwise it will be taken into account, so we have,

$$\langle \delta(k, \eta)\delta(k', \eta) \rangle = \langle \delta^{(1)}(k, \eta)\delta^{(1)}(k', \eta) \rangle + \langle \delta^{(2)}(k, \eta)\delta^{(2)}(k', \eta) \rangle + 2\langle \delta^{(1)}(k, \eta)\delta^{(3)}(k', \eta) \rangle + \dots \quad (3.60)$$

The non-linear correction can be obtained directly by inserting the solution. Thus, depending on truncated order after a finite number of terms, the non-linear regime can be exploited to provide better accuracy. However, in context of the perturbative expansion we would stop over in what is called 1-loop⁶ contribution, by the following expression,

$$\mathcal{P}_\delta(k, z) = \mathcal{P}_L(k, z) + \mathcal{P}_{1\text{-loop}}(k, z). \quad (3.61)$$

Being the contributions to the 1-loop,

$$\boxed{\mathcal{P}_{1\text{-loop}}(k, z) = 2\mathcal{P}_{(1,3)}(k, z) + \mathcal{P}_{(2,2)}(k, z)}. \quad (3.62)$$

For project purposes, the 1-loop contribution will be more than adequate and it is going to be relevant on reaction formalism due to it connects the non-linear regime with the modified halo model.

3.3 Halo model

In this section we aim to describe the standard halo model theory (see [Cooray & Sheth, 2002] for a review). This approach took inspiration from products of very large simulations (see e.g. **The Millennium Simulation Project** or **CAMELS**) that exhibit with a high-resolution the gravitational evolution of galaxies clustering and dark matter field, culminating in a cosmic web of filaments and nodes. Such nodes are deemed as **dark matter halos**, whose description is highly non-linear. In this model, the key assumption consists that all matter density is confined inside of those halos, then, the matter density at position \mathbf{x} is given by a superposition of each halo contribution as follows,

$$\rho_m(\mathbf{x}) = \sum_i^{\text{all halos}} \rho_h(\mathbf{x} - \mathbf{x}_i | M_i). \quad (3.63)$$

where \mathbf{x}_i is located at center-of-mass and M_i is the mass contained in the i -th halo. The following expressions depends on z , however, the redshift does not play a role in calculations, so we avoid it. Typically, density profile of the halo ρ_h is normalised as $u(\mathbf{x} - \mathbf{x}_i | M_i) \equiv \rho_h(\mathbf{x} - \mathbf{x}_i | M_i) / M_i$.

In the halo model, the fully non-linear matter power spectrum is composed by the sum of two terms,

$$\mathcal{P}(k) = \mathcal{P}_{1h}(k) + \mathcal{P}_{2h}(k). \quad (3.64)$$

The 1-halo involves the correlation by galaxy pairs within a single halo and dominates on small scales, whereas, the 2-halo term counts galaxy pairs from different halos and becomes important on large scales, see schematically Figure 3.2.

So now, let us focus on the 2PCF of (3.63),

$$\langle \rho_m(\mathbf{x}) \rho_m(\mathbf{x} + \mathbf{r}) \rangle = \sum_i \sum_j \langle M_i M_j u(\mathbf{x} - \mathbf{x}_i | M_i) u(\mathbf{x}_1 - \mathbf{x}_j | M_j) \rangle, \quad (3.65)$$

where $\mathbf{x}_1 = \mathbf{x} + \mathbf{r}$. We split this in two parts: if $i = j$ means 1-halo contributions otherwise $i \neq j$ is 2-halo. In integral form the 1-halo correlation function is written as:

$$\xi_{1h}(\mathbf{r}) = \langle \delta_m(\mathbf{x}) \delta_m(\mathbf{x} + \mathbf{r}) \rangle_{1h} = \int dM M^2 n(M) \times \langle u(\mathbf{x} - \mathbf{x}' | M) u(\mathbf{x}_1 - \mathbf{x}' | M) \rangle. \quad (3.66)$$

⁶The *loop* word involves a closely analogy of diagrammatic representation from quantum field theory.

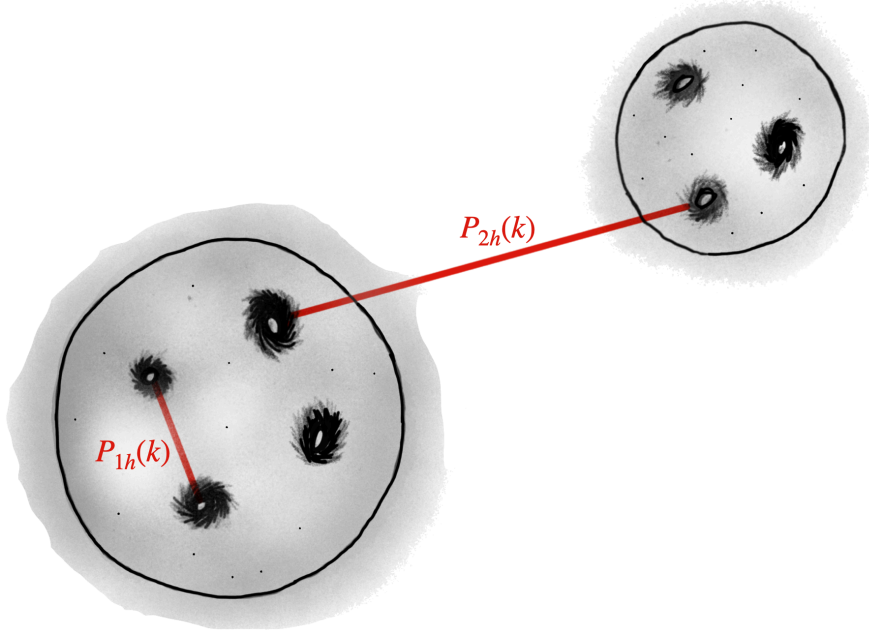


Figure 3.2: Illustration of the contributions to the halo model power spectrum. The $\mathcal{P}_{1h}(k)$ term considers correlations in isolated halos, while $\mathcal{P}_{2h}(k)$ term accounts for correlations between different halos. Image credits to Ivan Miranda.

We have introduced the halo mass function $n(M)$, which is a counting of the halos of mass M per volume unit.

$$\xi_{1h}(\mathbf{r}) = \frac{1}{\bar{\rho}^2} \int dM M^2 n(M) \int d^3x' u(\mathbf{x} - \mathbf{x}'|M) u(\mathbf{x}_1 - \mathbf{x}'|M). \quad (3.67)$$

Unlike 1-halo, in 2-halo the correlation comes from different halos, so this induces a linear halo bias $b(M)$. This means that halos are biased tracers of the underlying dark matter density field and are connected by the relation $\delta_h = b(M)\delta_m$. So, now the correlation function is given by,

$$\xi_{hh}(\mathbf{r}|M_1, M_2) = b(M_1)b(M_2)\xi_{\text{mm}}^L(\mathbf{r}), \quad (3.68)$$

where $\xi_{\text{mm}}^L(\mathbf{r})$ is the linear matter-matter 2PCF. This leads to obtain the 2PCF for the 2-halo term as,

$$\begin{aligned} \xi_{2h}(\mathbf{r}) = & \frac{1}{\bar{\rho}^2} \int dM_1 M_1^2 b(M_1) n(M_1) \int dM_2 M_2^2 b(M_2) n(M_2) \times \\ & \int d^3x' \int d^3x'' u(\mathbf{x} - \mathbf{x}'|M_1) u(\mathbf{x}_1 - \mathbf{x}''|M_2) \xi_{\text{mm}}^L(\mathbf{x}' - \mathbf{x}''). \end{aligned} \quad (3.69)$$

By spherical symmetry $u(\mathbf{x} - \mathbf{x}_i|M) = u(r, M)$. Finally, the 2PCFs (3.67) and (3.69) can be converted into terms of the power spectrum (3.64) through Fourier transform and returning the redshift dependency,

$$\mathcal{P}_{1h}(k, z) = \int_0^\infty dM n(M, z) \left(\frac{M}{\bar{\rho}} \right)^2 |u(k, M)|^2, \quad (3.70)$$

$$\mathcal{P}_{2h}(k, z) = \mathcal{P}_L(k, z) \left[\int_0^\infty dM n(M, z) \left(\frac{M}{\bar{\rho}} \right) b(M) u(k, M) \right]^2. \quad (3.71)$$

Where $u(k, M)$ corresponds to density profile in the Fourier space truncated at r_{vir} ,

$$u(k, M) = 4\pi \int_0^{r_{\text{vir}}} dr u(r, M) r^2 \text{sinc}(kr). \quad (3.72)$$

The cut-off r_{vir} is called virial radius, thus this set a spherical region with a mass,

$$M_{\text{vir}} = \frac{4\pi}{3} r_{\text{vir}}^3 \Delta_{\text{vir}} \bar{\rho}. \quad (3.73)$$

This represents the mass of the halo. The virial overdensity is given by,

$$\Delta_{\text{vir}} = [1 + \delta(a_{\text{vir}})] \left(\frac{a_{\text{col}}}{a_{\text{vir}}} \right)^3. \quad (3.74)$$

Since halos formed from regions in the initial density field which were sufficiently dense that they later collapsed, we are going to follow the evolution of a spherical top-hat overdensity in order to approximate the halo formation. We assume an initial condition at a_i as

$$\delta(r, a) = \left(\frac{r_i}{r} \right)^3 (1 + \delta_i) - 1. \quad (3.75)$$

Spherical Collapse.- In order to solve the non-linear collapse of a top-hat overdensity,

$$\rho = \begin{cases} \bar{\rho}(1 + \delta) & r \leq R, \\ \bar{\rho} & R \leq r. \end{cases} \quad (3.76)$$

We can relate (3.13) and (3.14) in order to obtain a second order equation (see, e.g., [Schmidt et al., 2009]). The evolution of the non-linear density results in,

$$\ddot{\delta} + 2H\dot{\delta} - \frac{4}{3} \frac{\delta^2}{(1 + \delta)} = \frac{(1 + \delta)}{a^2} \nabla^2 \Phi. \quad (3.77)$$

Lastly we could use (3.75) to get

$$\frac{\ddot{r}}{r} = -\frac{4\pi G}{3} [\bar{\rho}_{\text{CDM}} + (1 + 3\omega_{\text{DE}})\bar{\rho}_{\text{DE}}] - \frac{4\pi G}{3} \bar{\rho}_{\text{CDM}} \delta. \quad (3.78)$$

So, noticing we need to solve the spherical collapse in order determinate the virialised quantities.

Density profile.- In this approach the density profile of the dark matter halos is modelled through NFW (Navarro-Frenk-White) profiles,

$$u(r, M) = \frac{\rho_h(r, M)}{M} = \frac{\rho_s}{M} \frac{1}{(r/r_s)(1 + r/r_s)^2}, \quad (3.79)$$

where r_s is the separation between core-halo. The normalization constant ρ_s is obtained from integrating $M = \int dx^3 \rho_h(r, M)$, resulting that,

$$\rho_s = \rho_{\text{crit}} \frac{\Omega_m(z) \Delta_{\text{vir}}}{3} \left[\ln(1 + c) - \frac{c}{1 + c} \right]^{-1}. \quad (3.80)$$

In which allow us to define the concentration parameter $c \equiv r_{\text{vir}}/r_s$.

Halo mass function.- We denoted $n(M, z)$ as the comoving number density of bound halos which estimates the population of virialized dark matter halos. The comoving number density of halos with mass in the range $[M, M + dM]$ is given by:

$$n(M, z) \equiv \frac{dn}{d \ln M} = \bar{\rho} \nu f(\nu) \frac{d \ln \nu}{d \ln M}. \quad (3.81)$$

We have further defined the halo mass function $dn/d \ln M$, where ν is the peak-height and the function $\nu f(\nu)$ is known as the multiplicity function. A simple Gaussian distribution to adjust such function was provided by Press and Schechter, however, simulations have been applied to calibrate ([Sheth et al., 2001]) the halo mass function, hence, finding that the Sheth-Tormen distribution⁷ is more accurate than Press-Schechter, which is the following,

$$\nu f(\nu) = A \sqrt{\frac{2}{\pi}} q \nu^2 [1 + (q \nu^2)^{-p}] \exp(-q \nu^2 / 2). \quad (3.82)$$

The peak-height is $\nu \equiv \delta_{\text{sc}}^2 / \sigma^2(M, z)$, where δ_{sc} is the critical density from spherical halo collapse extrapolated to $z = 0$ and $\sigma^2(M, z)$ is the mass variance obtained from Eq. 3.57. The best fitted parameters from simulations is $A = 0.3222$, $q = 0.75$ and $p = 0.3$.

Concentration-mass relation.- To find the r_s value, the concentration-mass (c-M) relation is used,

$$c_{\text{vir}}(M_{\text{vir}}, z) = \frac{c_0}{1+z} \left(\frac{M_{\text{vir}}}{M_*} \right)^{-\alpha} \frac{f_{\text{DE}}(z \rightarrow \infty)}{f_{\Lambda\text{CDM}}(z \rightarrow \infty)}. \quad (3.83)$$

Fixing $c_0 = 0.9$ and $\alpha = 0.13$, and M_* is obtained by $\nu(M_*) = 1$.

Halo bias.- Lastly, as a result of considering Sheth-Tormen distribution, the peak-background split formalism predicts a linear halo bias as:

$$b(M) = 1 - \frac{1}{\delta_c} \left(1 - q \nu^2 + \frac{2p}{1 + (q \nu^2)^p} \right). \quad (3.84)$$

In light of simulations and observations this expression is also in well agreement (see [Sheth & Tormen, 1999]) with them.

We had obtained all components to calculate the fully non-linear spectra (3.64) within the Halo model approach for ΛCDM , nevertheless, we aim to extended this formalism to alternatives theories.

3.3.1 Halo model reaction

The halo model reaction formalism is an extension of the previous standard halo model but applied into beyond ΛCDM theories (see [Cataneo et al., 2019], [Bose et al., 2020] and [Cataneo, 2022]). The beyond ΛCDM non-linear spectrum $\mathcal{P}_{\text{NL}}(k, z)$ (denoted as “real”) is the product of the reaction $R(k, z)$ times a pseudo non-linear spectrum as follows

$$\mathcal{P}_{\text{NL}}^{\text{real}}(k, z) \equiv R(k, z) \cdot \mathcal{P}_{\text{NL}}^{\text{pseudo}}(k, z). \quad (3.85)$$

⁷Within this formalism is considered halos with an ellipticity.

The “pseudo” term refers a Λ CDM cosmology whose initial condition by exactly matching of $\mathcal{P}_L^{\text{real}}(k) = \mathcal{P}_L^{\text{pseudo}}(k)$ in order to target the modified cosmology. The reaction is defined as follows⁸:

$$R(k, z) = \frac{[(1 - \mathcal{E}) \exp(-k/k_*) + \mathcal{E}] \mathcal{P}_L^{\text{real}}(k, z) + \mathcal{P}_{1h}^{\text{real}}(k, z)}{\mathcal{P}_L^{\text{real}}(k, z) + \mathcal{P}_{1h}^{\text{pseudo}}(k, z)}. \quad (3.86)$$

Here k_* and \mathcal{E} are not free parameters. So, first the k_* scale is in charge of the transition rate from the linear to the non-linear scales, and is determined by solving at each redshift the following equation:

$$R(k_0, z) = \frac{\mathcal{P}_L^{\text{real}}(k_0, z) + \mathcal{P}_{1\text{-loop}}^{\text{real}}(k_0, z) + \mathcal{P}_{1h}^{\text{real}}(k_0, z)}{\mathcal{P}_L^{\text{pseudo}}(k_0, z) + \mathcal{P}_{1\text{-loop}}^{\text{pseudo}}(k_0, z) + \mathcal{P}_{1h}^{\text{pseudo}}(k_0, z)}. \quad (3.87)$$

Here the scale of $k_0 = 0.06 h/\text{Mpc}$ represents the maximum scale where CPT would be reliable. While $\mathcal{E}(z)$ is obtained via the limit,

$$\mathcal{E}(z) = \lim_{k \rightarrow 0} \frac{\mathcal{P}_{1h}^{\text{real}}(k, z)}{\mathcal{P}_{1h}^{\text{pseudo}}(k, z)}. \quad (3.88)$$

The behaviour of Eq. (3.86) on the spectrum is shown in Figure 3.3.

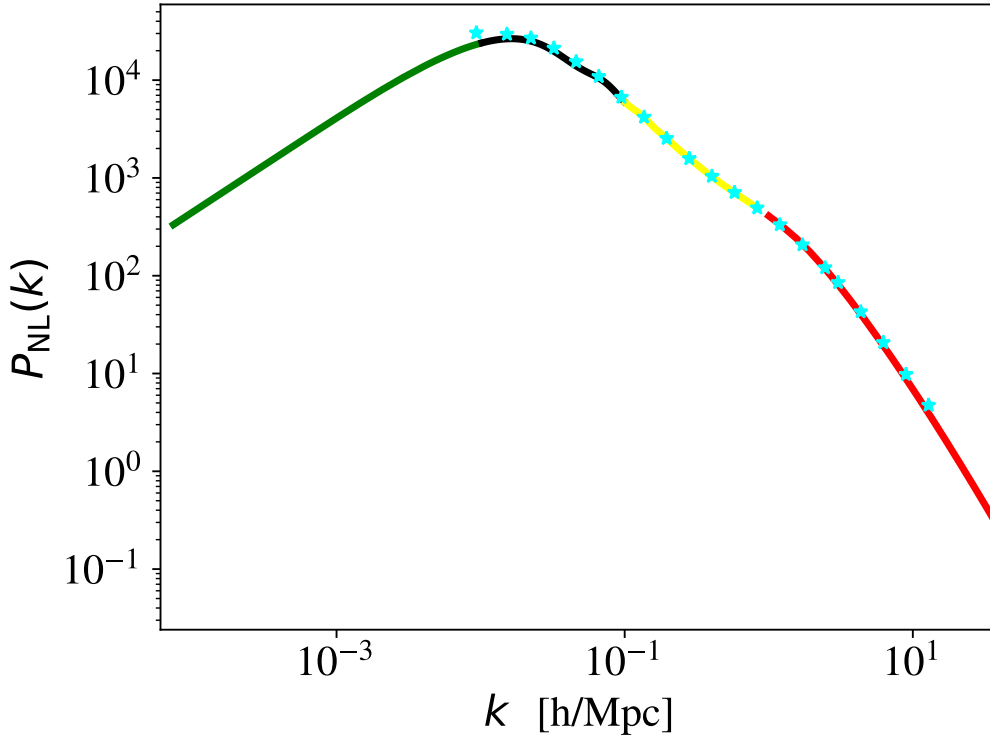


Figure 3.3: The halo model reaction behaviour on the spectrum (exemplified for a realization of the IDE model). In green, the range $k \leq 0.01 h/\text{Mpc}$ is primarily controlled by the linear spectrum, when, in Eq. (3.86), $R = 1$. The black line $0.01 h/\text{Mpc} \leq k \leq 0.1 h/\text{Mpc}$ is well described by CPT, while the yellow region $0.1 h/\text{Mpc} \leq k \leq 1 h/\text{Mpc}$ is controlled by the halo mass reaction function ratio. Finally, the rest of the scales in red ($k \geq 1 h/\text{Mpc}$) is approximated via $R \approx \mathcal{P}_{1h}^{\text{real}}/\mathcal{P}_{1h}^{\text{pseudo}}$. Note that there is an excellent match with the results of simulations, given by cyan stars.

In addition, the modifications on gravity enter directly through the Poisson equation.

⁸Notice that the 2-halo term is absent. According to [Cataneo et al., 2019], the improper integral in (3.71) can be set to unity without a measurable impact on the halo model reaction

$$\nabla^2\Phi = 4\pi G(1 + \mathcal{F}), \quad (3.89)$$

where \mathcal{F} encodes the information of modified theory. In summary, the reaction provides a new framework to map accurately the non-linear matter power spectrum in Λ CDM to other alternative theory (this is already tested on w CDM, CPL, $f(R)$ gravity and nDGP, see [Cataneo et al., 2019] for more details regarding the accuracy results).

3.4 Full spectra

In the previous sections, we have shown that we can model the matter power spectrum on non-linear scales through the halo model reaction. However that works only for dark matter, in order to get a full prediction for the matter power spectrum that is relevant for observations, we need to include the effects of baryon feedback and massive neutrinos, which substantially alter the power spectrum on small scales.

3.4.1 Presence of Neutrinos

Following Cataneo et al. [2020], massive neutrinos have been implemented to reaction formalism through their matter perturbations in the halo model (see also [Massara et al., 2014]). The sum of all matter contributions would be given by,

$$\delta_m = (f_c\delta_c + f_b\delta_b) + f_\nu\delta_\nu. \quad (3.90)$$

Being $f_a = \rho_a/\rho_m$. Since the matter power spectrum is proportional as $\mathcal{P} \propto \delta_m^2$, then it reads as,

$$\mathcal{P}^{(m)}(k) = (1 - f_\nu)^2\mathcal{P}^{(cb)}(k) + 2f_\nu(1 - f_\nu)\mathcal{P}^{(cb\nu)}(k) + f_\nu^2\mathcal{P}^{(\nu)}(k), \quad (3.91)$$

where $(m) = (cb + \nu)$ establishes the sum of CDM (c), baryons (b) and neutrinos (ν). Given that, the formula of the reaction $\mathcal{R}(k, z)$ with massive neutrinos now is written as the following form,

$$\mathcal{R}(k) = \frac{(1 - f_\nu)^2\mathcal{P}_{\text{HM}}^{(cb)}(k) + 2f_\nu(1 - f_\nu)^2\mathcal{P}_{\text{HM}}^{(cb\nu)}(k) + f_\nu^2\mathcal{P}_{\text{L}}^{(\nu)}(k)}{\mathcal{P}_{\text{L}}^{(m)}(k) + \mathcal{P}_{\text{1h}}^{\text{pseudo}}(k)}, \quad (3.92)$$

with $\mathcal{P}_{\text{HM}}^{(0)} = [(1 - \mathcal{E})\exp(-k/k_\star) + \mathcal{E}]\mathcal{P}_{\text{L}}^{(0)} + \mathcal{P}_{\text{1h}}^{(0)}$.

3.4.2 Baryonic feedback

For a complete description of the non-linear matter spectrum, we resort to include the contributions caused by the baryons within the Active Galactic Nuclei (AGN) surrounded by dark matter halo. Building through the standard halo model prescription ([Chisari et al., 2019]), the baryonic model encodes 6 parameters that takes into account effects from AGN feedback and star formation. However, that model was fitted to the BAHAMAS simulations [McCarthy et al., 2017] to obtain a 1-parameter model, which depends only on the temperature of AGN, via $\theta \equiv \log_{10}(T_{\text{AGN}}/\text{K})$. Such baryonic feedback is taken into account by an extra boost factor, $\mathcal{B}(k, z)$, defined by the ratio between the full power spectrum and the DM-only spectrum, as follows,

$$\mathcal{B}(k, z) = \frac{\mathcal{P}_{\text{full}}}{\mathcal{P}_{\text{c}}}. \quad (3.93)$$

Therefore, to obtain a full power spectrum within the halo model reaction framework, we combine baryonic and reaction prescriptions to obtain,

$$\mathcal{P}_{\text{NL}}(k, z) = \mathcal{R}(k, z) \cdot \mathcal{B}(k, z) \cdot \mathcal{P}_c^{\text{pseudo}}(k, z). \quad (3.94)$$

With this prescription we can readily predict the non-linear matter power spectrum in the presence of baryon feedback effects.

3.5 Interacting Dark Energy models

In the realm of the Λ CDM model, the dark matter and dark energy always remain uncoupled. Theoretically, nothing prohibits to allow the gravitationally interaction between these dark components⁹. This captivating statement sheds light to model interacting dark energy (IDE) with dark matter, although there is a rich selection about the kind of interaction (e.g. interacting scalars field, interacting fluids, interacting in $f(R)$ and so forth), these models have been the key to explain some irregularities that currently occur in the Λ CDM model, for example, the coincidence problem (see [Caldera-Cabral et al., 2009]) or to alleviate the data tension, particularly with S_8 , which is the growth rate of the structure (see [Carrilho, Moretti, & Pourtsidou, 2022], [Di Valentino et al., 2017], [Mancini Spurio & Pourtsidou, 2022]). The addition of the dark interaction can slow down the growth of dark matter density fluctuations, thus reducing their amplitude at late times.

The coupling is modelled by a current Q^ν that represents the energy and momentum exchange between dark energy and dark matter, therefore, the energy-momentum tensors of dark matter and dark energy are no longer separately conserved,

$$\nabla_\mu T_c^{\mu\nu} = Q^\nu, \quad \iff \quad \nabla_\mu T_{\text{DE}}^{\mu\nu} = -Q^\nu. \quad (3.95)$$

Nonetheless, the total momentum-energy tensor is clearly conserved, $\nabla_\mu T_c^{\mu\nu} + \nabla_\mu T_{\text{DE}}^{\mu\nu} = 0$. A formal approach of describing the coupled dark sector is through the Lagrangian,

$$\mathcal{L} = -\frac{1}{2}g^{\mu\nu}\partial_\mu\phi\partial_\nu\phi - V(\phi) - m(\phi)\bar{\psi}\psi + \mathcal{L}[\psi], \quad (3.96)$$

where ϕ is an evolving scalar field of the dark energy named **quintessence** and ψ is considered as a scalar field dark matter (SFDM) with a mass¹⁰ $m(\phi)$, in this approach the coupling current is defined as,

$$Q_\nu \equiv \rho_c \partial_\nu \phi \frac{\partial \ln m(\phi)}{\partial \phi}. \quad (3.97)$$

The form of the coupling current is a phenomenological choice. Now, focusing on the background contribution of $\bar{Q}^\nu \rightarrow (Q_0(\eta), 0, 0, 0)$, resulting the equation for SFDM as,

$$\frac{\partial \bar{\rho}_c}{\partial \eta} + 3H\bar{\rho}_c = Q_0, \quad (3.98)$$

and for DE equation as,

$$\frac{\partial \bar{\rho}_\phi}{\partial \eta} + 3H\bar{\rho}_{\text{DE}}(\omega_{\text{DE}} + 1) = -Q_0, \quad (3.99)$$

where the form Q_0 is fairly diversified (see e.g. [Caldera-Cabral et al., 2009], [Bertolami et al., 2012], [Tarrant et al., 2012], [Amendola et al., 2012]). However, the most popular IDE models are

⁹Note that this statement assumes the standard model is not coupled to the dark sector.

¹⁰If the mass depends only on the SFDM there would be no interaction with DE, i.e. only a self-interaction.

just described by a ϕ -quintessence explicitly coupled to pressure-less DM, i.e CDM. The coupling could be simple (only 1 extra parameter) such that permits to adapt well to CMB or LSS data due to its simplicity. This project will be involved in such models within the pull-back formalism (see [Pourtsidou et al., 2013] for details) in the GR framework coupled to an adiabatic fluid. In this context this description might provide fundamental insights at the level of the action on how such coupling could emerge in order to built general models of coupled IDE with the aim by exploring whether those models has a limit to phenomenological case or not. The total action has the form,

$$S = \int d^4x \sqrt{-g} R - \int d^4x \sqrt{-g} \mathcal{L}(n, \phi, X, Z), \quad (3.100)$$

in which n is the CDM number density, $X = \frac{1}{2}g^{\mu\nu}\partial_\mu\phi\partial_\nu\phi$ is the kinetic term and $Z = u^\mu\nabla_\mu\phi$ is the coupling of the CDM velocity to the gradient of ϕ . Doing the variation on the action (3.100), where we have

$$\delta\mathcal{L} = \frac{\partial\mathcal{L}}{\partial n}\delta n + \frac{\partial\mathcal{L}}{\partial\phi}\delta\phi + \frac{\partial\mathcal{L}}{\partial X}\delta X + \frac{\partial\mathcal{L}}{\partial Z}\delta Z. \quad (3.101)$$

- Varying with the scalar field: $\frac{\delta\mathcal{S}}{\delta\phi} = 0$. One would obtain the equations of the scalar field,

$$\nabla_\mu \left(\frac{\partial\mathcal{L}}{\partial X}\nabla_\mu\phi + \frac{\partial\mathcal{L}}{\partial Z}u_\mu \right) = \frac{\partial\mathcal{L}}{\partial\phi} \quad (3.102)$$

- Varying with the metric: $\frac{\delta\mathcal{S}}{\delta g_{\mu\nu}} = 0$, resulting in Einstein equations with the total energy-momentum tensor as,

$$T_{\mu\nu} = \frac{\partial\mathcal{L}}{\partial X}\partial_\mu\phi\partial_\nu\phi + \left(n\frac{\partial\mathcal{L}}{\partial n} - Z\frac{\partial\mathcal{L}}{\partial Z} \right) u_\mu u_\nu + \left(n\frac{\partial\mathcal{L}}{\partial n} - \mathcal{L} \right) g_{\mu\nu}. \quad (3.103)$$

- Varying with the number density: $\frac{\delta\mathcal{S}}{\delta n} = 0$. We find the conservation law of the fluids,

$$\nabla_\mu(nu^\mu) = 0. \quad (3.104)$$

According to Pourtsidou et al. [2013], with the above equations in hand these IDE models can be further classified via three types from their Lagrangian $\mathcal{L} = F + f$, where F stands for ϕ -quintessence contributions and f is for CDM contributions.

Type I.- The Lagrangian of these models does not depend on Z and has the following convenient separated form:

$$\mathcal{L} = F(X, \phi) + f(n, \phi) = X + V(\phi) + f(n, \phi). \quad (3.105)$$

The CDM density and pressure can be identified by Eq. (3.2) like,

$$\rho_c = f, \quad P_c = n\frac{\partial f}{\partial n} - f = 0. \quad (3.106)$$

Being set $f(n, \phi) = n \exp[\alpha(\phi)]$, where $\alpha(\phi)$ is a free function. From the Eq (3.102), in Type I case the scalar field equation becomes,

$$\nabla_\mu \left(\frac{\partial F}{\partial X} \partial_\mu \phi \right) = \frac{\partial \mathcal{L}}{\partial \phi} + \rho \frac{\partial \alpha}{\partial \phi}. \quad (3.107)$$

From the Eq (3.103), we only obtain the energy-momentum tensor for ϕ ,

$$T_{\mu\nu}^{(\phi)} = \frac{\partial F}{\partial X} \partial_\mu \phi \partial_\nu \phi - F g_{\mu\nu}. \quad (3.108)$$

Hence, coupling current is given by $Q_\nu = -\nabla_\mu T_\nu^{(\phi)\mu}$, then we find that,

$$Q_\nu^{(I)} = -\rho_c \frac{\partial \alpha}{\partial \phi} \nabla_\nu \phi, \quad (3.109)$$

where we have made use of Eqs. (3.107) and (3.108). This coupling involves the transfer of energy and momentum.

Type II.- The coupling of these models introduces a transfer of energy and momentum as well due to the energy-momentum tensors are shared from the Type I case. The Lagrangian is set as follows,

$$\mathcal{L} = F(X, \phi) + f(n, Z) = X + V(\phi) + f(n, Z). \quad (3.110)$$

While $f(n, Z) = nh(Z)$. Unlike before, it is introduced a new coupling function $\beta(Z)$, which is obtained via $h(Z) = \exp\left(\int ds \frac{\beta}{1+\beta s}\right)$ in order to follow a similar proceed of the previous case, thus, we find the coupling current like,

$$Q_\nu^{(II)} = \nabla_\mu (\rho_c \beta u^\mu) \nabla_\nu \phi. \quad (3.111)$$

With density term as $\rho_c = f - Z \frac{\partial f}{\partial Z}$.

Type III.- Lastly, these class of models will be part of our interest for this project, their coupling is set through the following Lagrangian:

$$\mathcal{L} = F(X, Z, \phi) + f(n) = X + V(\phi) + Z + f(n). \quad (3.112)$$

Likewise, we again follow a similar proceed in order to find the coupling current, resulting in

$$Q_\nu^{(III)} = -\nabla_\mu \left(\frac{\partial F}{\partial Z} u^\mu \right) \hat{\phi}_\nu + \frac{\partial F}{\partial Z} D_\nu Z + Z \frac{\partial F}{\partial Z} u^\mu \nabla_\mu u_\nu. \quad (3.113)$$

Here the projector tensor $q_{\mu\nu}$ was used into $D_\nu = q_\mu^\nu \nabla_\nu$ and $\hat{\phi}_\nu = D_\nu \phi$. Surprisingly, type 3 models are particularly special because their coupling involves pure transfer of momentum and highlighting no coupling $\hat{Q} = 0$ at the background level.

3.5.1 Dark Scattering

Throughout the development of the PhD project, the model we are interested in studying is named as **Dark Scattering** (DS) model (first explored by Simpson [2010]), consisting of an analogy with Thomson's scattering between electrons and photons by identifying dark sector species like,

$$\mathbf{Q}_T = -\frac{4}{3}\sigma_T a \rho_\gamma n_e (\mathbf{u}_e - \mathbf{u}_\gamma), \quad (3.114)$$

$$\downarrow$$

$$\mathbf{Q}_{\text{DS}} = -(1 + w_{\text{DE}})\sigma_{\text{DS}} a \rho_{\text{DE}} n_c (\mathbf{u}_c - \mathbf{u}_{\text{DE}}). \quad (3.115)$$

This is an elastic interaction that assumes the pure exchange of momentum exclusively between the perturbations of the dark sector. Therefore, it might be part of Type III models but we are going to discuss it later in this section. In the meantime let us define the interaction term as follows,

$$A \equiv \xi (1 + w_{\text{DE}}) \frac{3\Omega_{\text{DE}}}{8\pi G} H. \quad (3.116)$$

Clearly, the strength of the interaction term depends on background quantities and parameter $\xi \equiv \sigma_{\text{DS}}/m_c \geq 0$ in units [b/GeV], where σ_{DS} is the interaction cross section and m_c is CDM particle mass. Moreover, DS model can be considered as an extension of w CDM models, and also has a well-defined limit Λ CDM when $w_{\text{DE}} \rightarrow -1$ we have $A = 0$, see Figure 3.4.

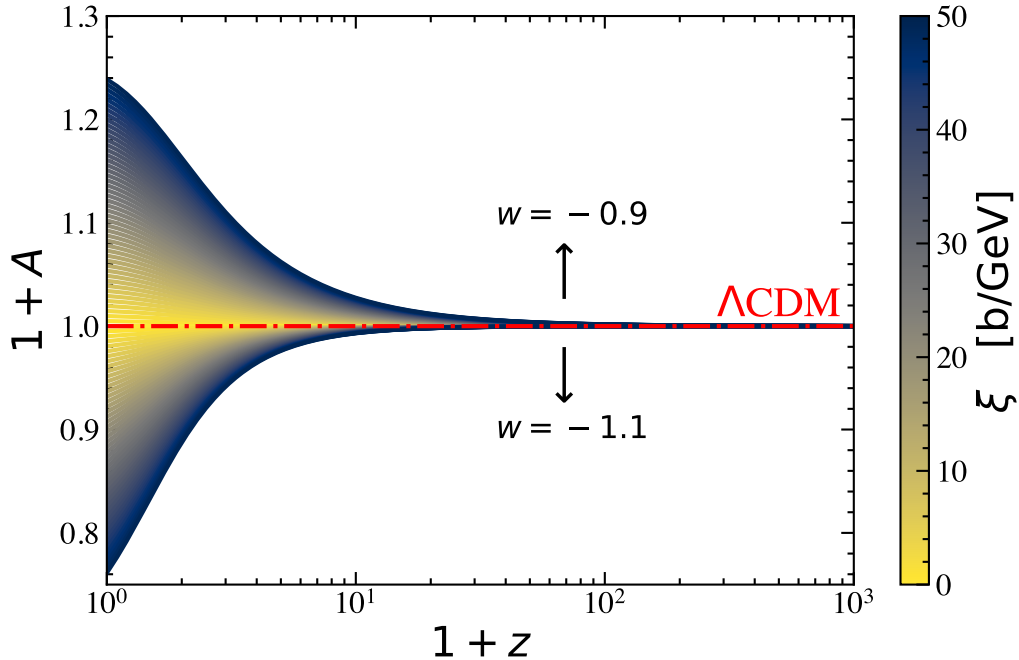


Figure 3.4: Interaction strength ξ as a function of redshift, for a range of constant equation of state parameter values.

The DS formulation has been simulated to the non-linear level in Baldi & Simpson [2015] for different values of the coupling parameter ξ and Baldi & Simpson [2017] considered modified cosmologies, as result of that the interaction is always linear in the dark matter velocity, therefore allowing us to extrapolate its effect for the equation of motion of individual particles as

$$\dot{\mathbf{u}} = -(1 + A)H\mathbf{u} - \nabla_{\mathbf{r}}\Phi. \quad (3.117)$$

Remarkably, the effect of the interaction acts as an additional frictional force on the CDM of dragging or expanding, depending on $\text{sign}(A)$.

As we mentioned above, the DS interaction only implies CDM velocity and not its density, then this model could be mapped to a subset of Type III models. In Baldi & Simpson [2017] was showed that this could be done approximately, by assuming a Lagrangian of the type $F \propto \exp(-Z)$. Alternatively, Skordis et al. [2015] developed a parametrisation based on Post-Friedmann approach

in order to introduce all possible type of terms that can appear in a coupled theory by reducing the large parameter space of free functions and coupling types to small set of constants.

Parameterised Post-Friedmann.- The Parameterised Post-Friedmann (PPF) formalism consists of linearised the perturbations of the coupling current $Q^\nu = \bar{Q}^\nu + \delta Q^\nu$ which are separated in these variables,

$$q \equiv \delta Q_0, \quad \text{and} \quad \nabla_i S \equiv \delta Q_i. \quad (3.118)$$

Turning them now to a linear combination of all other perturbations (fluid and metric variables) with new coefficients A_n , B_n and C_n . In addition obeying gauge transformations and making use of gauge invariants, this can be extended into general description for generalized fields (see [Skordis et al., 2015] for full expressions). Nonetheless, for project purposes we remain in the special case of CDM and the Dark Energy fluid under Newtonian gauge, thus the expressions are reduced into,

$$q = Q_0\Psi - 6A_1\Phi - 6A_2(\dot{\Phi} + \mathcal{H}\Psi) + A_3\delta_{\text{DE}} + A_4\delta_c + A_5\theta_{\text{DE}} + A_6\theta_c, \quad (3.119)$$

$$S = -6B_1\Phi - 6B_2(\dot{\Phi} + \mathcal{H}\Psi) + B_3\delta_{\text{DE}} + B_4\delta_c + B_5\theta_{\text{DE}} + B_6\theta_c. \quad (3.120)$$

In this context the coupling current of Type III models (3.113) takes the following form,

$$\mathbf{Q}^{(\text{III})} = B_3\nabla\delta_{\text{DE}} + B_5\mathbf{u}_{\text{DE}} + B_6\mathbf{u}_c. \quad (3.121)$$

Whereas $A_n = 0$ and $Q_0^{(\text{III})} = 0$, we would expect that, since the Type III models produce couplings of pure momentum exchange up-to linear order in CPT. On the other hand, the DS coupling current (3.115) requires $B_3 = 0$, as a consequence DS coupling would not be possible to map exactly to Type III because fixing $B_3 = 0$ translates to set F independent of Z (i.e. $\frac{\partial F}{\partial Z} = 0$). In other words from (3.113) results, it is clearly to see that the model becomes completely uncoupled.

Not all is lost, however, we still can connect DS model to Type III case by considering the sound speed $c_s^2 = 1$, therefore, DE perturbations could be vanished $\delta_{\text{DE}} = \mathbf{u}_{\text{DE}} = 0$, so that, making those type 3 models have a similar form to the DS case (see [Baldi & Simpson, 2017]). While just remaining the time-dependence of B_6 that can be matched as,

$$B_6 = -(1 + w_{\text{DE}})\sigma_{\text{DS}}a\rho_{\text{DE}}n_c. \quad (3.122)$$

SPECIFIC OBJECTIVES

In this brief chapter, the project objectives will be sequentially exposed.

Completed work

1. From Section 3.2, one objective of this project is extending the CPT (see e.g. [Aviles & Cervantes-Cota, 2017]), particularly to the domain of DS model from subsection 3.5.1, and then implementing the required modifications in the halo model reaction in order to compute the DS non-linear matter power spectrum.
2. Subsequently, we sought a validation for our power spectrum prediction, to do that, we compared products of simulations (from [Baldi & Simpson, 2017]) to our halo model reaction prediction provided by the code `ReACT` which has been implemented in the DS contributions.
3. At the level of the full spectrum in Eq. (3.94), now we focused on determining whether a degeneracy exists between DS and baryonic feedback parameters. Likewise, we assert whether the neutrino effects can mimic the interaction contribution. To that end, we attempted to fit a non-interacting model with varying baryonic/neutrinos feedback to an interacting model with fixed baryonic/neutrinos feedback.

Ongoing work

1. Furthermore, we are planning to make use of `ReACT` to generate thousands of DS non-linear spectra ($\sim 10^5$) as a training set in order to create an accelerated trained emulator. Such DS emulator is provided by `CosmoPower`, a tool that is based on Machine Learning.
2. Adapting these fast emulators to cosmology is a novel technique for statistical purposes. In order to estimate and infer parameters in a more efficient way of working in cosmo-statistics, hence, we want to integrate the DS emulator in our pipeline by using the bayesian analysis code called `Cobaya`.

Future work

1. The bayesian analysis will be oriented to describe clustering and lensing observables with simulated (Euclid-like) and real data from the KiDS-1000 ([Heymans et al., 2021]).
2. Consequently, employing the Bayesian Evidence for different DE equations of state within the DS model in order to pin down which model is more preferable by the data.
3. Despite these can be used for galaxy clustering studies (see [Moresco et al., 2022] for more extensions), it further can be turned to 21cm intensity maps. The use of `CosmoPower` might allow to generate, for example, a quick 21cm power spectrum prediction by interpolating training data.
4. Lastly, we plan to explore the Power Spectrum Multipoles expansion for H_I intensity mapping following e.g [Poursidou, 2022] and [Cunnington et al., 2020].

METHODOLOGY AND REQUIRED TECHNIQUES

Now we show the computational tools needed to reach our specific objectives.

5.1 Methodology

A deep understanding of CPT, halo model and IDE are essential to lead the way on the use of sophisticated statistical tools, emulators, and simulations for this project. This PhD project builds on the tools and expertise available and aims at providing novel tools and results that will be useful for forthcoming cosmological surveys. Furthermore this project stipulates a dedicated program of training on the use of state-of-the-art computational and statistical tools. The sequence of methods is as follows:

5.1.1 Simulations and dataset

Unfortunately at full non-linear level, our modelling does not converge to the real evolution of inhomogeneities, and it is thus necessary resort to the N-body or hydrodynamical cosmological simulations. Motivated by that, one main methodology within this project was the validation of our power spectrum prediction against cosmological N-body simulations and exploring their deviations from Λ CDM.

Parameter	Value
h	0.678
Ω_c	0.2598
Ω_b	0.0482
\mathcal{A}_s	2.115×10^{-9}
n_s	0.966

Table 5.1: Our baseline cosmological parameters.

To measure power spectra, we have worked with available N-body simulations products provided by Marco Baldi. They were performed by a modified version of the GADGET-2 [Springel, 2005]. Moreover, all simulations share the base cosmological parameters given in Table 5.1 and were set up to 1024^3 CDM particles evaluated at $z_i = 99$ and trace it up to $z = 0$ within a box of 1 Gpc/ h per side. Additionally, they all share the same initial seeds so that we can divide-out cosmic variance by taking ratios of power spectra (see [Baldi & Simpson, 2017] for a more extended description of the simulations).

5.2 ReACT

Recently Bose et al. [2020] have written the reaction formalism in a publicly available C++ code, called `ReACT`. In addition, the code has the advantage of including a Python wrapper, which allow us to run `ReACT` within Python interpreter (e.g. Jupyter notebook). In order to obtain the reaction, `ReACT` requires an input that has the cosmological model parameters in Table 5.1, takes the linear power spectrum provided by `CAMB` or `CLASS` and the modified theory with its respective extra parameters, see the flowchart in Figure 5.1 for details.

Pseudo spectrum.- Since the pseudo spectrum is based on Λ CDM model that follows the standard halo model approach. Then, the pseudo power spectrum can be obtained via `HMCCode` [Mead et al., 2021]. The required inputs are the value of $\sigma_8(z=0)$ derived from the cosmological parameters and also the linear spectrum given by `CLASS` ([Lesgourgues, 2011]) or `CAMB` ([Lewis et al., 2000]).

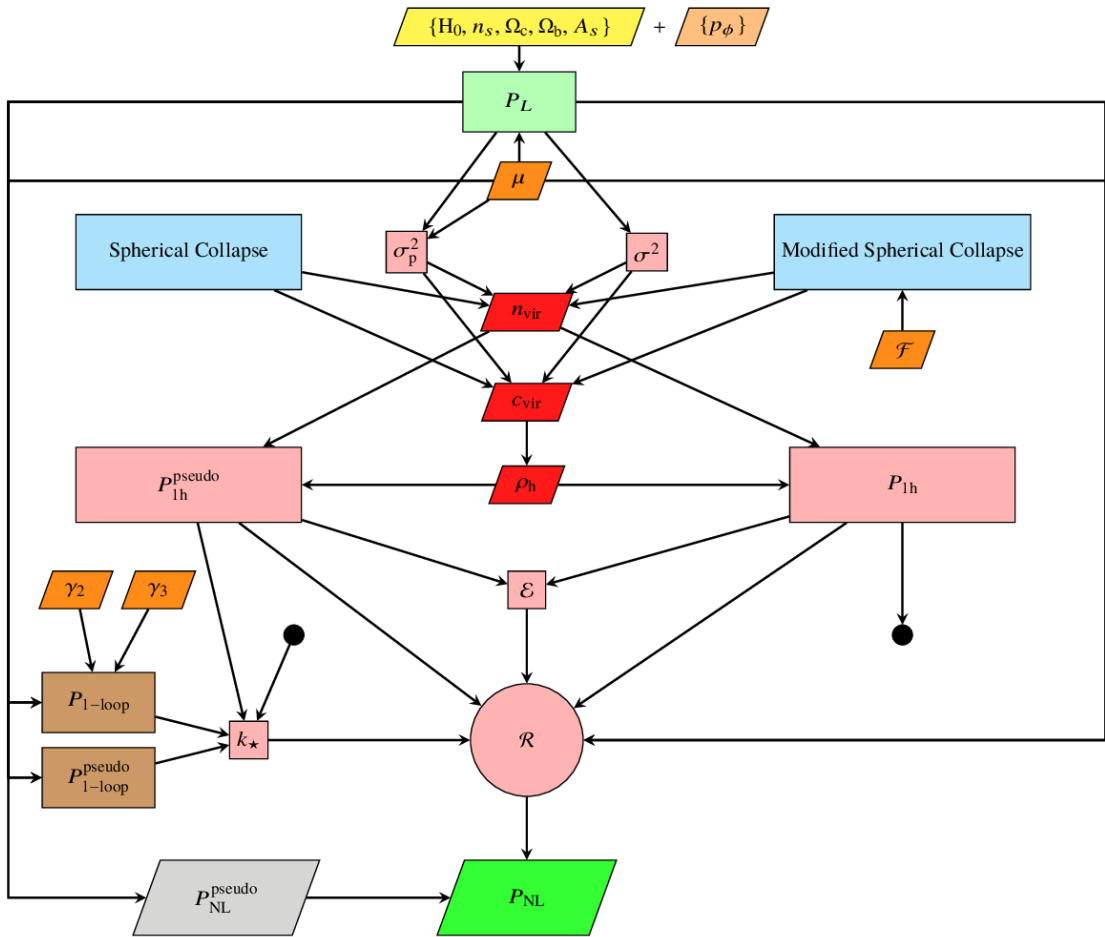


Figure 5.1: An overview of the computation of the non-linear power spectrum in `ReACT`, discussed in the text. Image taken from [Bose et al., 2020].

In [Bose et al., 2021] has proven the reaction by using `ReACT` to be a method capable to reach an accuracy of 5% against simulations at $k < 10$ h/Mpc and more recently ([Bose et al., 2022]) by improving to 2%. Here a modification of `ReACT` will be presented, where the effects of the DS will be included by modulating the parameter ξ . In spirit of [Bose et al., 2021], we also plan to include the effects generated from baryon feedback and massive neutrinos.

5.2.1 ReACT with neutrinos + baryons

Neutrinos.- Currently, the inclusion of neutrino in reaction (3.92) has been added in ReACT (see [Bose et al., 2021]). The effects of neutrinos are modulated through their mass: $M_\nu = \sum_i^{N_\nu} m_{\nu_i} \sim N_\nu \bar{m}_\nu$. Their contribution on the energy budget of the Universe is,

$$\Omega_\nu = \frac{M_\nu}{93.14h^2}. \quad (5.1)$$

Massive neutrinos induce a suppression on the power spectrum, since they do not cluster as efficiently as cold matter on sufficiently small scales (see [Agarwal & Feldman, 2011]).

Baryons.- For this case we include the effects of baryonic feedback in the computation of the pseudo power spectrum. As we mentioned before, the baryonic model is modulated through the temperature of AGN: $\theta \equiv \log_{10}(T_{\text{AGN}}/K)$, and was validated in the range $7.6 \leq \theta \leq 8.3$ (see [Mead et al., 2021] for more details). The module that provides the baryonic boost (3.93) is available within the interfaz of `HMCode2020_feedback`.

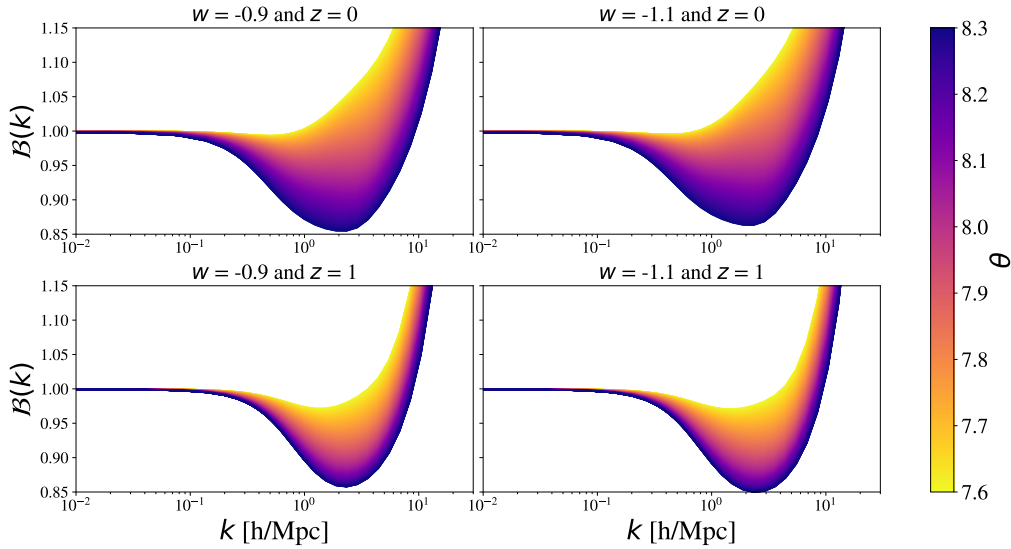


Figure 5.2: The variation of the feedback parameter θ in the colorbar. The effects on the $\mathcal{B}(k)$ of w CDM cosmology at $z = 0$ (top) and $z = 1$ (bottom). Note that at intermediate scales, the feedback shows a suppression of power, while for non-linear scales it is a booster.

The baryonic feedback induces suppression on the power spectrum on intermediate scales, due to gas expulsion from AGN feedback, and an enhancement on smaller scales due to star formation, as is shown in Figure 5.2.

5.3 CosmoPower

Nowadays, the implementation of Neuronal Networks (NN) for machine learning techniques on frontier science has had an impressive impact, and their utilization on cosmology is not lagging behind. During this stage, I have been learning to use `CosmoPower`, which is a Python-based library for Machine Learning. This code helps to emulate the power spectra through a trained NN with a very high-dimensional parameter spaces. The trained thing is so-called **emulator** that might be replacing Boltzmann codes (either `CLASS` or `CAMB`), since they easily generates spectra much faster than Boltzmann codes. Consequently, this novel technique also promise to accelerate

Bayesian inference by orders-of-magnitude (see e.g. [Spurio Mancini et al., 2022] for CMB and LSS analysis by using Λ CDM emulators and in [Mancini Spurio & Pourtsidou, 2022] used an IDE emulator for weak lensing analysis).

Currently, `CosmoPower` permits only two methods to create a trained NN for emulating matter or CMB spectra. Firstly `cosmopower_NN`, see Figure 5.3, where the n -nodes of NN are set in a sequential hidden layers to learn in how to map between cosmological parameters and power spectra (similar to classify images) by associating them a weight W_n and bias parameter b_n , whose linear combination is passed through a non-linear activation function (see [Mancini Spurio & Pourtsidou, 2022] for details on the activation function). Secondly, `cosmopower_PCAplusNN` incorporates the Principal Component Analysis (PCA) method to match coefficients of the power spectra. Although, at least for our purposes we will employ the first method.

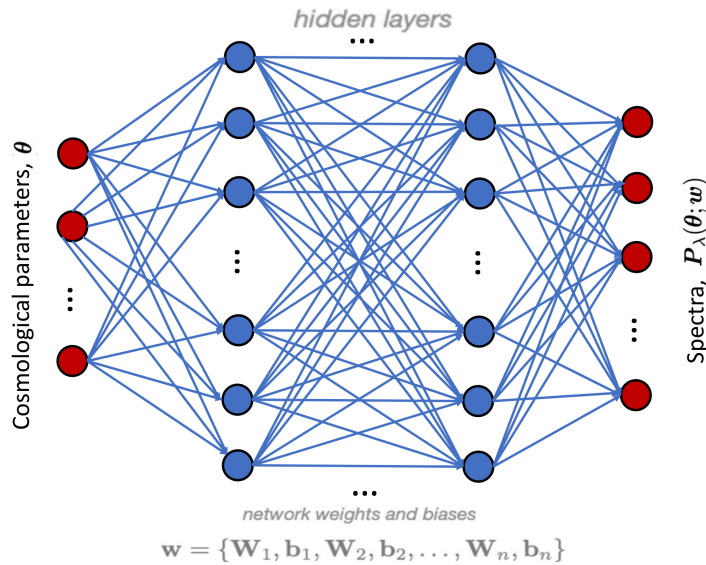



Figure 5.3: The routine of `cosmopower_NN`. The NN is composed by a set of stacked layers, each composed of multiple nodes (blue circles). The input cosmological parameters are mapping to the spectra $\mathcal{P}_\lambda(\theta; w)$, so that, the NN learns through the non-linear activation function. Image taken from `CosmoPower` .

In a nutshell, `CosmoPower` basically requires a training set of the cosmological parameters θ and the associated training set of log-power spectra. The outcome trained emulator can be also tested to validate its accuracy which depends on the number of samples for training.

5.4 Cobaya

In order to perform a cosmological parameter estimation, we use an user-friendly code for bayesian analysis known as `Cobaya` (**C**ode for **b**ayesian **a**nalysis), which has been adapted from other sources, such as `CosmoMC` and `MultiNest`. In statistical framework, `Cobaya` permits to explore our priors and likelihoods by performing just a likelihood evaluation (this is useful for testing) or a Markov Chain Monte Carlo (MCMC) (using a advanced MCMC sampler from `CosmoMC`) or nested sampling (see [Ashton et al., 2022]) with a sampler called `PolyChord`. In addition, it is included automatic installers for using cosmological codes¹ `CAMB` or `CLASS`, as well as likelihoods of cosmological experiments, such as `Planck`, `SDSS`, `DES` among others. It also supports MPI parallelization.

¹This is very convenient for including in a modified version of them.

The information in the input that Cobaya reads is contained in a text file based on *YAML* format, which consists of a Python dictionary specifying 5 different blocks: **theory**, **likelihood**, **params**, **sampler** and **output**, with various options in each block. Here is an input example of considering DES year 1 data ([Abbott et al., 2018]) in the likelihood, also setting CLASS and MCMC sampler:

```

1 theory:
2   classy:
3     path: ./class_public
4     extra_args:
5       non linear: hmcode
6       N_ncdm: 1
7       N_ur: 2.0328
8
9 likelihood:
10    #DES Y1 -- Clustering data
11    des_y1.clustering:
12      path: ./Clustering/data/des_data
13    des_y1.shear:
14      path: ./Shear/data/des_data
15    des_y1.galaxy_galaxy:
16      path: ./Galaxy/data/des_data
17
18 params:
19   logA:
20     prior:
21       min: 2.97
22       max: 3.11
23     ref:
24       dist: norm
25       loc: 3.05
26       scale: 0.001
27     latex: \log(10^{10} A_{\mathrm{s}})
28     drop: true
29
30   A_s:
31     value: 'lambda logA: 1e-10*np.exp(logA)'
32     latex: A_{\mathrm{s}}
33
34   n_s:
35     prior:
36       min: 0.94
37       max: 0.98
38     ref:
39       dist: norm
40       loc: 0.965
41       scale: 0.004
42     latex: n_{\mathrm{s}}
43
44   H0:

```









```

45     prior:
46         min: 67
47         max: 69
48     latex: H_0
49
50     omega_b:
51         prior:
52             min: 0.02
53             max: 0.025
54         ref:
55             dist: norm
56             loc: 0.02212
57             scale: 0.0005
58         latex: \Omega_{\mathrm{b}} h^2
59
60     omega_cdm:
61         prior:
62             min: 0.12
63             max: 0.15
64         ref:
65             dist: norm
66             loc: 0.1206
67             scale: 0.001
68         latex: \Omega_{\mathrm{cdm}} h^2
69
70     sampler:
71         mcmc:
72             #Number of discarded burn-in samples
73             burn_in: 10000
74
75             #Maximum number of accepted steps
76             max_samples: .inf
77
78             # - "auto" (cosmology runs only): will be looked up in a library
79             covmat: auto
80
81             #Convergence checks of the MCMC run.
82             #Gelman-Rubin R-1 on means
83             Rminus1_stop: 0.01
84
85             #Gelman-Rubin R-1 on std deviations
86             Rminus1_cl_stop: 0.2
87
88             #A second check is also performed on the bounds of
89             #the Rminus1_cl_level \% confidence level interval.
90             Rminus1_cl_level: 0.95
91
92     output: chains/cosmo_mcmc

```

Afterwards the posteriors of the sampling can be analysed with `GetDist`.

The relevant softwares mentioned in this section are publicly available:

- The linear spectrum can be obtained from either CLASS  or CAMB .
- The version included the DS modification in ReACT .
- The modified DS linear spectrum from DS-CLASS .
- The DM-only pseudo power spectrum and the baryonic feedback correction are provided by the HMCode .
- The emulators generator CosmoPower .
- For statistical analysis is Cobaya .
- The advanced nested sampler is Polychord .

PROGRESS

The most relevant progress so far in the PhD project is separated by sections below.

6.1 Implementation of the DS in ReACT

We aim to incorporate the DS formulation of subsection 3.5.1 into the code ReACT afterwards as we mentioned before we will validate our modelling against simulations products from [Baldi & Simpson, 2017]. Following [Baldi & Simpson, 2015], the equation of motion in terms of our perturbations variables (subtracting the background) with considering a new friction term is given by,

$$\frac{\partial \mathbf{p}}{\partial \eta} = -A\mathcal{H}\mathbf{p} - ma\nabla_{\mathbf{x}}\Phi, \quad (6.1)$$

which is quite similar to that one from (3.7) just by an extra interacting term. Hence, we just follow-up the previous steps done in Section 3.2 in order to re-acquire the evolution equations for dark sector fluctuations. At zeroth-order moment

$$\frac{\partial \delta}{\partial \eta} + \nabla_{\mathbf{x}} \cdot [(1 + \delta)\mathbf{u}] = 0 \quad (6.2)$$

Surprisingly, noticing that the Continuity equation is unaltered by the interaction. Followed by the Euler equations,

$$\frac{\partial u_j}{\partial \eta} + u_i \nabla_{x_i} u_j + \mathcal{H}u_j + \nabla_{x_j} \Phi + \frac{1}{\rho} \nabla_{x_i} (\sigma_{ij}) = -A\mathcal{H}u_j. \quad (6.3)$$

Simplifying, we finally obtain the second order non-linear equation for δ that we are looking for,

$$\underbrace{\ddot{\delta}}_{\text{Acceleration}} + \underbrace{(2H + A)\dot{\delta}}_{\text{Friction}} - \frac{4}{3} \frac{\dot{\delta}^2}{(1 + \delta)} = \frac{(1 + \delta)}{a^2} \underbrace{\nabla^2 \Phi}_{\text{Force}}. \quad (6.4)$$

Noticing that the interacting term has appeared and acting like friction term. Furthermore, we can reduce it at linear order and changing into Fourier space

$$\ddot{\delta} + (2H + A)\dot{\delta} = \frac{1}{a^2} \nabla^2 \Phi. \quad (6.5)$$

Then we are able to modify the spherical collapse as,

$$\frac{\ddot{r}}{r} + AH\frac{\dot{r}}{r} = -\frac{4\pi G}{3} [\bar{\rho}_c + (1 + 3\omega)\bar{\rho}_{\text{DE}}] + AH^2 - \frac{4\pi G}{3} \bar{\rho}_c \delta. \quad (6.6)$$

As shown previously, the effect of the dark sector interaction is to generate an additional friction force on dark matter particles. Within the approximations used in this work, this friction force is clearly not conservative and it cannot be included in the traditional potential term of the virial

theorem. Therefore, we must add a non-conservative force $\mathbf{F}^{\text{fric}} = -mAH\mathbf{x}'_i$ to the standard expression

$$2\langle T \rangle + \langle W \rangle + \sum_i^{\text{all particles}} \langle \mathbf{F}_i^{\text{fric}} \cdot \mathbf{r}_i \rangle = 0, \quad (6.7)$$

where T is the total kinetic energy and W is the potential term of the system. Following [Cataneo et al., 2019], we write the contributions to the Virial theorem in terms of the normalised comoving radius $y \equiv (r/r_i) - (a/a_i)$ and in units of $E_0 \equiv \frac{3}{10}M(H_0r_i)^2$. The expressions in this case are:

$$\frac{W_N}{E_0} = -\Omega_m \left(\frac{a^{-1}}{a_i^2} \right) y^2 (1 + \delta), \quad (6.8)$$

$$\frac{W_{\text{DE}}}{E_0} = -\frac{H^2}{H_0^2} (1 + 3w_{\text{DE}}) \Omega_{\text{DE}} \left(\frac{a}{a_i} \right)^2 y^2, \quad (6.9)$$

$$\frac{W_{\text{DS}}}{E_0} = -2A \frac{H^2}{H_0^2} \left(\frac{a}{a_i} \right)^2 y \frac{dy}{d \ln a}. \quad (6.10)$$

For completeness, we present also the total kinetic energy of the top hat, T ,

$$\frac{T}{E_0} = \frac{H^2}{H_0^2} \left[\frac{a}{a_i} \left(\frac{dy}{d \ln a} + y \right) \right]^2. \quad (6.11)$$

To summarize, the equation that must be solved to find the virialisation time a_{vir} , as well as the corresponding overdensity Δ_{vir} , is

$$2T + W_N + W_{\text{DE}} + W_{\text{DS}} = 0. \quad (6.12)$$

Regarding including other non-CDM species in our modelling, one expects the effective strength of the interaction to be modulated by the dark matter fraction of the total matter, $f_c = \rho_c/\rho_m$. To explore that we split those species into CDM and non-CDM at the linear level, with the latter including baryons and massive neutrinos. We then define the total matter velocity divergence $\theta_m \equiv f_c \theta_c + f_{b\nu} \theta_{b\nu}$ and the velocity difference $\Delta\theta \equiv \theta_c - \theta_{b\nu}$. Since $\Delta\theta$ is expected to be small, we can approximate the solution for the $\Delta\theta$ equation by its equilibrium solution (i.e. the solution which gives $\Delta\theta' = 0$), that yields into the next equation,

$$\theta'_m = -\mathcal{H} \left(1 + \frac{A f_c}{1 + A f_{b\nu}} \right) \theta_m - \nabla^2 \Phi. \quad (6.13)$$

This demonstrates that the total matter evolves with an effective coupling function that depends on the relative amount of dark matter in the Universe. While this coupling function has a slightly modified time-dependence relative to the standard coupling function, A , we have verified with a numerical solution from our modified version of CLASS that it is a very good approximation to evaluate the denominator at $z = 0$, so that we can define an effective coupling constant $\bar{\xi}$, given by

$$\bar{\xi} = \frac{f_c}{1 + A_0(1 - f_c)} \xi. \quad (6.14)$$

At the non-linear level, this approximation assumes that we can put together the clustering species when computing the halo model prediction by using this effective coupling. These modifications are then applied to the calculation of the halo model reaction using ReACT. Then, this results in predictions for the DS non-linear power spectrum that can be compared to simulations. We perform this validation in the next section.

6.2 Validation of DS modelling

In Table 6.1 is summarised a subset of the simulations presented in [Baldi & Simpson, 2017] in which there are three models: Λ CDM, w CDM and CPL with a different ξ interaction strength. We must look for deviations from Λ CDM model in order to ensure that alternatives are well tested, to avoid false detections.

Model	w_0	w_a	ξ [b/GeV]	$\sigma_8(z=0)$
Λ CDM	-1.0	0.0	0	0.8261
w CDM+	-0.9	0.0	10	0.7939
w CDM-	-1.1	0.0	10	0.8512
CPL	-1.1	0.3	50	0.7898

Table 6.1: A summary of the simulations tested for validation.

w CDM + DS case.- We begin by validating our results for the cases of w CDM in Figure 6.1, where we show the ratio between the power spectra for the Dark Scattering model and the corresponding Λ CDM model at three redshifts in comparison with simulation measurements. Evidently, we place our reaction predictions within a modified version of `ReACT` in which the DS model is implemented for cosmologies with $w_0 = -0.9$ and $w_0 = -1.1$, the cosmological parameters of Table 5.1 and a coupling parameter value of $\xi = 10$ b/GeV. While the pseudo power spectra were obtained by `HMCode` that takes as input the linear power spectrum provided by `CAMB`.

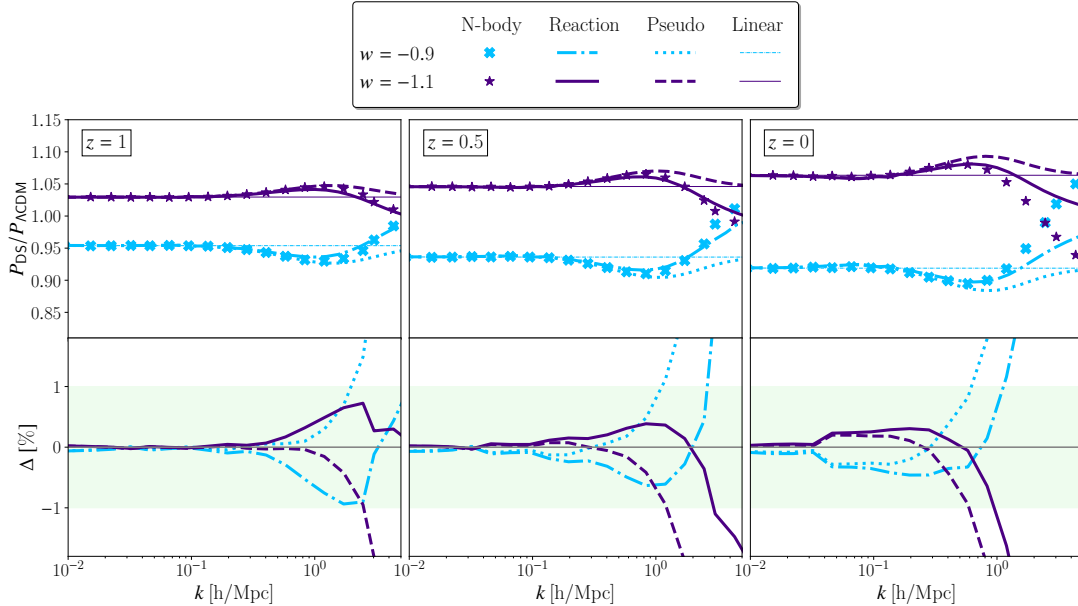


Figure 6.1: **Top:** Ratios of Dark Scattering spectra to Λ CDM, for a coupling strength of $\xi = 10$ b/GeV. The blue curves are for $w_0 = -0.9$, where crosses, dash-dotted lines, dotted lines and thin dashed-lines are measurements from simulations, the halo model reaction prediction, the pseudo spectrum prediction and the linear theory prediction, respectively. In purple, we show the results for $w_0 = -1.1$ where the same quantities as before are represented. **Bottom:** The residuals in percentage, $\Delta = 100\% \cdot \left(1 - \hat{P}_{\text{prediction}}/\hat{P}_{\text{N-body}}\right)$, for the reaction and pseudo spectrum predictions, where $\hat{P} = \mathcal{P}_{\text{DS}}/\mathcal{P}_{\Lambda\text{CDM}}$ is the ratio shown in the top plot.

As it can be inferred from Eq. (3.116) the interaction parameter A depends on whether the value of w lies above or below -1 . Provoking that these two cases have opposite effects; the case $w_0 = -0.9$ ($A > 0$) impacts in a suppression over Λ CDM spectrum, whereas $w_0 = -1.1$ ($A < 0$) results in an enhancement at intermediate scales. Unlike on highly non-linear scales, in which presents much stronger and opposite effect, as the additional friction for $w > -1$ causes structures to lose energy and collapse to deeper potential wells, thus forming denser structures, with the inverse happening for $w < -1$.

In addition as seen in Figure 6.1, at linear scales the effects of the DS are appreciable, on the other hand the non-linear are fairly small within the scales that we model accurately. This is particularly true at $z = 0$, where the size of the effect is sub-percent at $k < 1$ h/Mpc. Ignoring the interaction in the calculation of the reaction typically doubles the errors relative to simulations around $k \sim 1$ h/Mpc. Due to the non-linear effects arise both from the pseudo spectrum and from the reaction. With the large linear effects, the pseudo spectrum shows enhanced non-linear effects on intermediate scales, which are then compensated by the reaction. Thus, even when the interaction produces non-linear effects that are small, their modelling is only accurate when the coupling is fully taken into account.

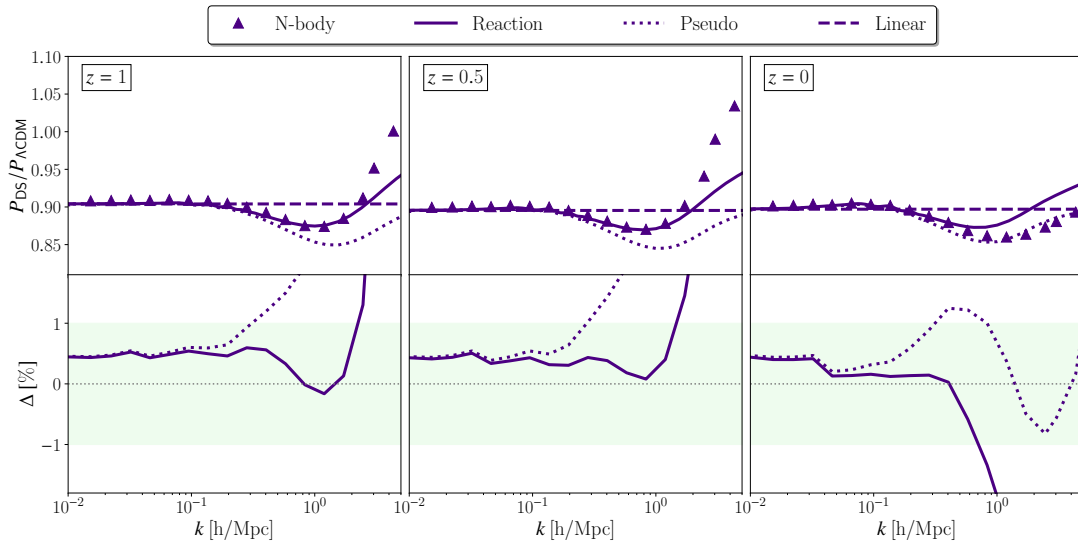


Figure 6.2: Top: Ratio of Dark Scattering spectrum (CPL: $w_0 = -1.1, w_a = 0.3$) with a value of $\xi = 50$ b/GeV to Λ CDM. Points are measurements from the simulations whereas solid lines are the halo model reaction prediction. Dotted lines are the pseudo spectrum and dashed lines are the linear theory prediction. **Bottom:** The residuals, as defined in Figure 6.1, for the reaction and pseudo spectrum predictions. Note that there is a sustained 0.5% discrepancy on large scales. The reason for this is that the N-body simulations ([Baldi & Simpson, 2017]) have been found to capture linear growth with differing accuracy depending on the value of ξ , so that the ratio between DS and Λ CDM is slightly modified with respect to the prediction. This is noticeable here and not in Figure 6.1, because of the much larger coupling.

CPL + DS case.- Afterwards, we validate the CPL parametrisation with a varying equation of state. We show our results for that case with $w_0 = -1.1, w_a = 0.3$ and $\xi = 50$ b/GeV at $z = 0, 0.5, 1$ in Figure 6.2. This case is interesting because the effective coupling, A , changes sign at $z = 0.5$, first being positive and suppressing linear growth at high redshift, and later enhancing it as redshift goes to 0. The biggest difference comes in the form of a change of shape on the smallest scales, visible in the results at $z = 0$, at which the interaction dampened most of the previous non-linear

amplification. All of these non-linear effects are enhanced here because we study the much larger interaction strength of $\xi = 50$ b/GeV. In spite of this, the prediction of the halo model reaction is 1% accurate up to scales of $k \approx 0.8$ h/Mpc at $z = 0$, reaching $k \approx 1.5$ h/Mpc at higher redshift. In addition, at $z = 0$, the errors are never larger than 4% for the entire range of scales available from the simulations.

In summary, the fact that our predictions are accurate for a substantial range of scales and redshifts, particularly for large interaction strengths, demonstrates that the reaction formalism is effective at modelling the non-linear effects of DS and can be used for the analysis of real data to constrain the interaction strength. For that to be fully realised, however, we need to understand all the contributions to the power spectrum on small scales, including those generated by baryon feedback and massive neutrinos. We analyse that in the next section.

6.3 Including baryons and neutrinos

Throughout this section, we employ the effective coupling approximation of (6.14), as there would be no realistic scenario for which only CDM is present.

Neutrinos degeneracy.- We now aim to investigate the degeneracy between massive neutrinos and the dark sector interaction. The effect of massive neutrinos is fully included in the reaction formalism in Eq. (3.92), and available implemented in `ReACT`. Here, we isolate the scale-dependent non-linear effects that we are interested in, instead of comparing the full power spectra, we match instead spectra normalized to their large scale value as,

$$Q_{\text{NL}} \equiv \frac{\mathcal{P}_{\text{NL}}}{\mathcal{P}_{\text{NL}}(k_*)}, \quad (6.15)$$

where $k_* \ll k_{\text{NL}}$ so that $\mathcal{P}_{\text{NL}}(k_*) \approx \mathcal{P}_{\text{L}}(k_*)$.

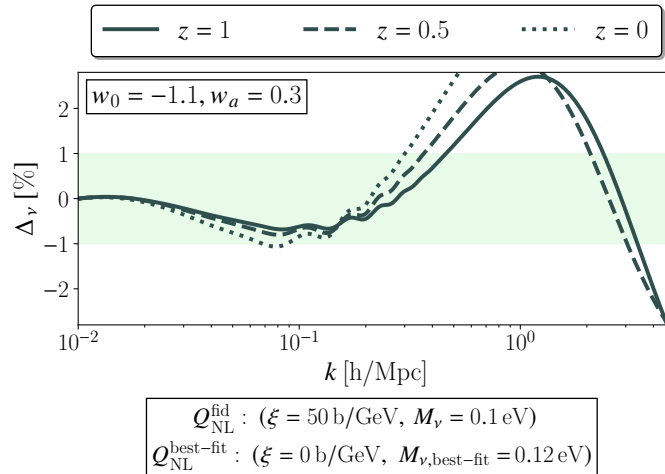


Figure 6.3: Residuals of the comparison between the Dark Scattering predictions for $\bar{\xi} = 50$ b/GeV ($\xi = 60$ b/GeV), $M_\nu = 0.1$ eV and the non-interacting case with a suitable neutrino mass (best-fit case: $M_{\nu, \text{best-fit}} = 0.12$ eV), at three different redshifts $z = 1$ (solid), $z = 0.5$ (dashed), and $z = 0$ (dotted). All plots pertain the CPL case: $w_0 = -1.1$, $w_a = 0.3$. The residual is defined by $\Delta_\nu = 100 \% \cdot (1 - Q_{\text{NL}}^{\text{fid}}/Q_{\text{NL}}^{\text{best-fit}})$.

We begin by considering a fiducial spectrum with $\bar{\xi} = 50$ b/GeV ($\xi = 60$ b/GeV), $w_0 = -1.1$, $w_a = 0.3$, we then generate results with no-interaction ($\xi = 0$), while varying neutrino mass

until we are able to find a value $M_{\nu, \text{best-fit}}$ which minimises the residuals between this case and the fiducial spectra. We fit all three redshift bins together and we consider only the scales for which our predictions from the halo model reaction have an accuracy of $\Delta \leq 1\%$ (displayed in Figure 6.2), ensuring that the neutrino contribution is not mimicking incorrect effects, which is shown in Figure 6.3. We found a neutrino mass of $M_{\nu} = 0.12$ eV with absence of interaction in the dark sector, that best fits the fiducial. We clearly see that a dark sector momentum exchange at the level of $\bar{\xi} = 50$ b/GeV cannot be mimicked by massive neutrinos alone, even if a single redshift slice is considered in isolation, therefore the case of massive neutrinos, no significant degeneracy is found. However, it should be remarked that we use a single set of dark energy parameters to test both degeneracies, and it is conceivable that a very different dark energy evolution would change these conclusions.

Baryonic feedback degeneracy.- We proceed in the same way as before, attempting to find a value for the baryonic feedback for which Q_{NL} mimics that of the interacting cosmology. We consider again our fiducial spectrum with $\bar{\xi} = 50$ b/GeV ($\xi = 60$ b/GeV), $w_0 = -1.1$, $w_a = 0.3$, adding a baryon boost with $\theta = 7.8$ and thus computing $Q_{\text{NL}}^{\text{fid}}$.

The results from this procedure are illustrated in Figure 6.4, where we show the residuals between the fiducial and best fit cases. As seen there the best-fit value is $\theta_{\text{best-fit}} = 8.01$, which is substantially different from the fiducial value of 7.8. It is also clear in the figure that modulating the feedback strength can mimic the effect of the interaction, as it reduced the residuals to below 1% on scales up to $k = 1$ h/Mpc, in which we trust our modelling fully.

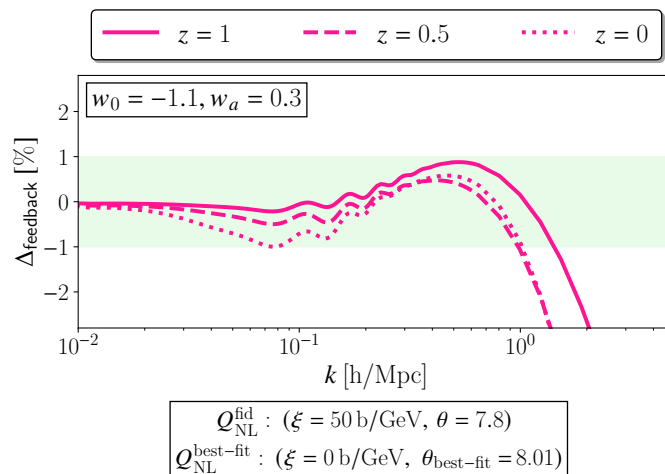


Figure 6.4: Residuals of the comparison between the Dark Scattering predictions for $\bar{\xi} = 50$ b/GeV ($\xi = 60$ b/GeV), $\theta = 7.8$ and the non-interacting case with the best-fit baryonic feedback ($\theta_{\text{best-fit}} = 8.01$), at three different redshifts $z = 1$ (solid), $z = 0.5$ (dashed), and $z = 0$ (dotted). In all cases we consider the CPL case: $w_0 = -1.1$, $w_a = 0.3$. The residual is defined by $\Delta_{\text{feedback}} = 100\% \cdot (1 - Q_{\text{NL}}^{\text{fid}}/Q_{\text{NL}}^{\text{best-fit}})$.

While these simplified tests already reveal some potential degeneracies between baryons feedback and DS effects, a more thorough MCMC analysis would enable us to exactly pin them down, as well as allowing us to fully validate our non-linear modelling. The presence of this degeneracy highlights the importance of using a combined analysis with spectroscopic clustering to constrain IDE (as analysed by Carrilho et al. [2021]), as their relative independence of baryonic feedback would help in breaking this degeneracy. We aim to fully explore that with photometric surveys in next stages of this project, where we will also be able to precisely define the range of applicability of our modeling as well as forecast the observability of the DS effects shown here.

6.4 First publication

As a result of the previous progress, during the first year of the PhD program, I collaborated as a co-author on an article publication (see [Carrilho, Carrion, et al., 2022]) based on the validation results. In this article, we generated the DM-only pseudo power spectrum from a Python-based code called `EuclidEmulator2` ([Knabenhans et al., 2021]) by giving as input a scalar amplitude A_s , corrected by the appropriate growth factors using `evogrowthpy`, i.e. $D_{\text{DS}}^2(z)/D_{\text{ACDM}}^2(z)$, thus ensuring the match to the linear power spectrum of the DS case, resulting in being slightly more accurate than `HMCODE` on intermediate scales. The article is already published in an international journal with arbitration.

6.5 Creating a fast DS emulator

In light of a well validation against simulations with percent-level accuracy of DS non-linear spectrum. We plan now to create a DS emulator trained by `CosmoPower`.

In order to get familiar with `CosmoPower`, as a first test, I successfully created a DS CMB emulator C_ℓ^{DS} . Then, we considered next to make a pipeline in order to generate DS non-linear spectra from `ReACT`. Such pipeline is parametrised in terms of just 9 parameters, given by,

$$\theta_{\text{DS}} = \{\Omega_b, \Omega_{\text{cdm}}, n_s, \ln 10^{10} A_s, h, w_0, \xi, m_\nu, z\}. \quad (6.16)$$

We considered a 5σ interval of the cosmological parameters from Planck 2018 ([Aghanim et al., 2020]) best-fit, as follows,

Parameter	Range of validity
Ω_b	[0.0477, 0.04890]
Ω_{cdm}	[0.2830, 0.3391]
h	[0.6556, 0.6975]
n_s	[0.9475, 0.9855]
$\ln 10^{10} A_s$	[2.977, 3.117]
m_ν	[0, 0.2] eV
w_0	[-0.85, -1.15]
ξ	[0, 20] b/GeV
z	[0, 5]

Table 6.2: The range of validity of the DS emulator.

So, I had to resort to parallelization methods to generate 150,000 spectra samples by separating them $\sim 90\%$ for training and $\sim 10\%$ for testing. Here, I want to acknowledge the usage of Chacaltzingo, a computing cluster from ICF-UNAM facilities, in which I make use of 10 CPU cores and the Python package called `multiprocessing` to generate the spectra samples. Afterwards, we prepared our NN, then the samples for training are passed through the four hidden layers. Then, the trained DS emulator was put in testing against the testing samples, resulting in a desired accuracy as is shown in Figure 6.5.

While using `ReACT` to generate 10^5 samples took around 5 days by parallelising into 10 CPU cores, the DS emulator just needs ~ 1 minute and that is incredibly impressive. For that reason, our purposes for the DS power spectra emulator is to implement it into the bayessian analysis by considering real cosmological data from experiments or simulated data, in contemplation of being tested against the accuracy requirements for the analysis of next-generation cosmological surveys.

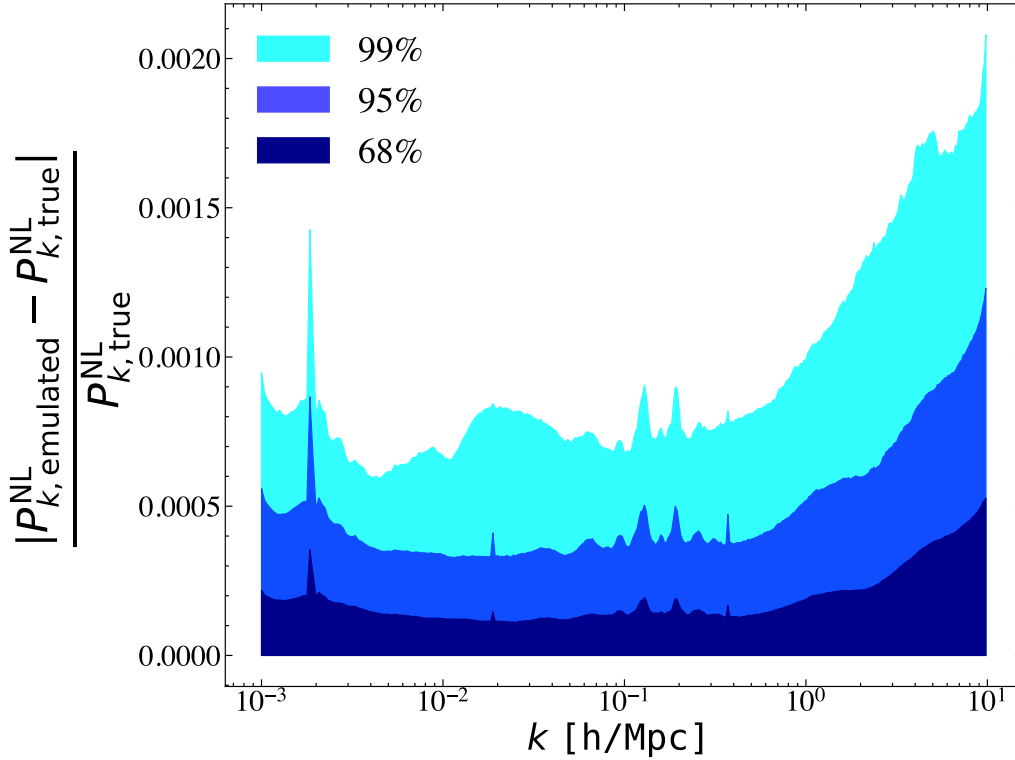


Figure 6.5: Preliminary accuracy of the first DS emulator against 2×10^4 spectra of the testing set. The dark blue, blue and cyan areas enclose the 68, 95 and 99 percentiles of the fractional absolute emulator error, respectively.

6.6 Adapting Cobaya to emulators

Our motivation now is the fact that, in cosmology, an accurate parameter estimation are turning very expensive. For example, in a typical MCMC the power spectra provided by Boltzmann codes are evaluated more than 10^4 on the likelihood, thus the runtime requires a long time. This has led to the replacement of the Boltzmann codes to emulators in order to speed-up the inference pipeline.

In this stage, I implemented in `Cobaya` a Λ CDM emulator of CMB spectra which works with the six parameters:

$$\theta_{\Lambda\text{CDM}} = \{\Omega_b h^2, \Omega_{\text{cdm}} h^2, h, \tau_{\text{reio}}, n_s, \ln 10^{10} A_s\}. \quad (6.17)$$

Subsequently, I employed a MCMC analysis by considering the Planck 2018 likelihood incorporated within `Cobaya`, resulting in Figure 6.6, where the convergence of Gelman-Rubin criterion of 0.01 value is reached. Afterwards, in Figure 6.7 I compare Λ CDM linear emulator to `CLASS` by using a DES year 1 likelihood of clustering.

Currently, I have been working on creating a better DS emulator for non-linear spectrum that contains a wider range of parameters, here I acknowledge use of the Cuillin computing cluster of the Royal Observatory, University of Edinburgh.

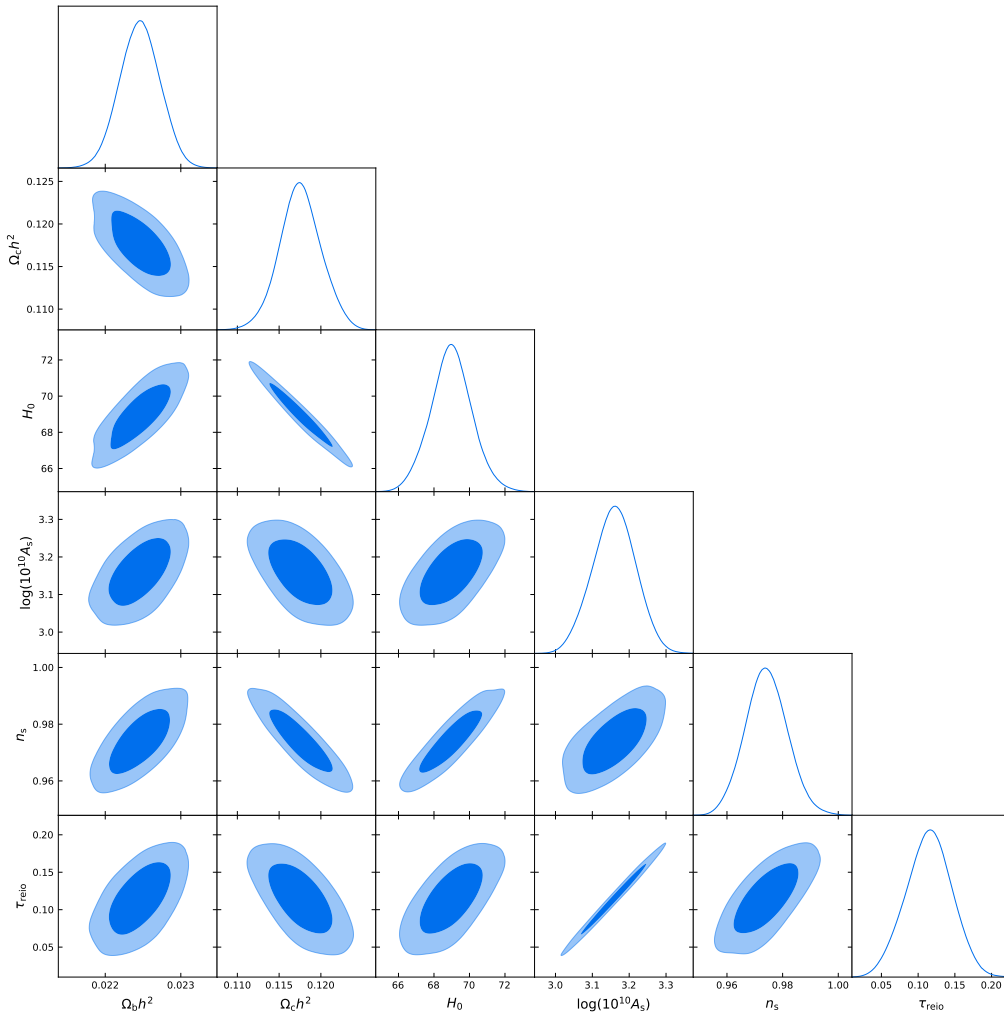


Figure 6.6: Implementation of the CMB emulator in Cobaya , where I reproduced posteriors similar to those from the paper [Spurio Mancini et al., 2022] as a first test.

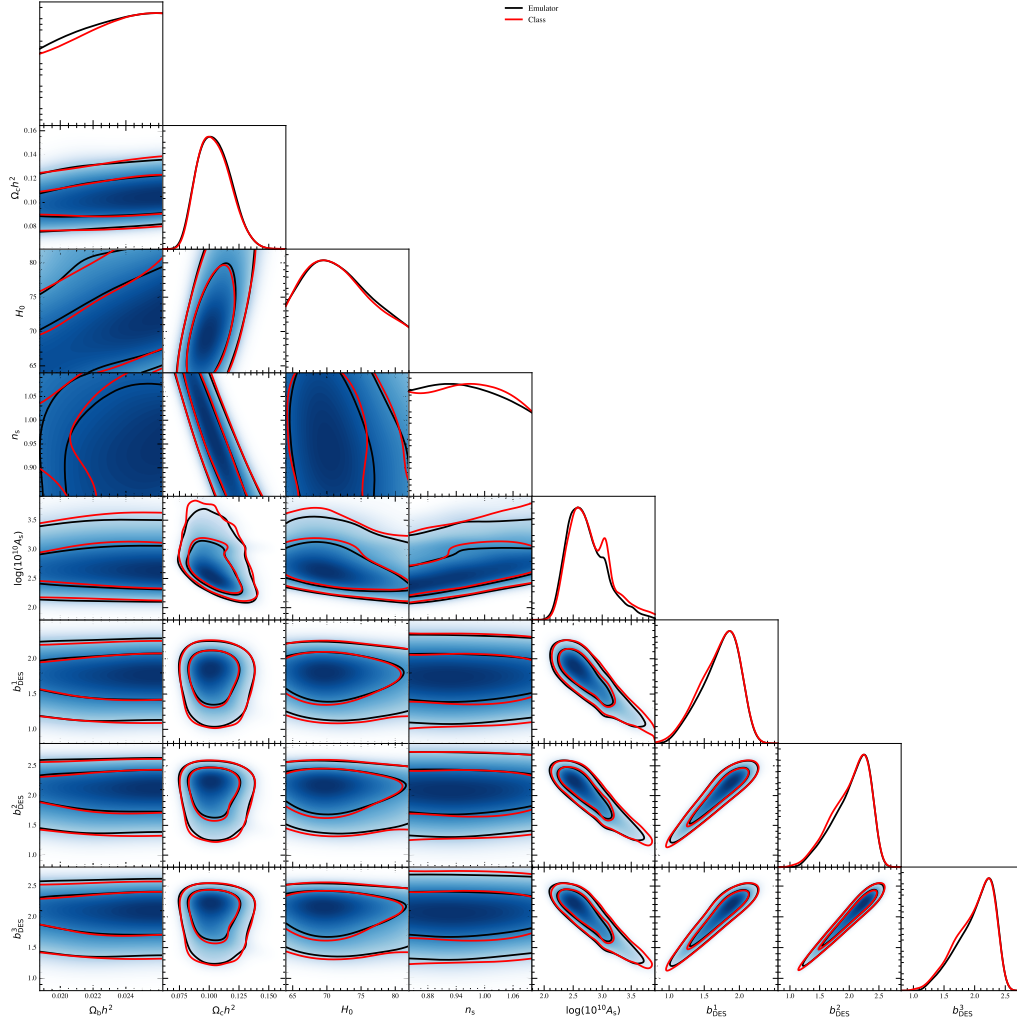
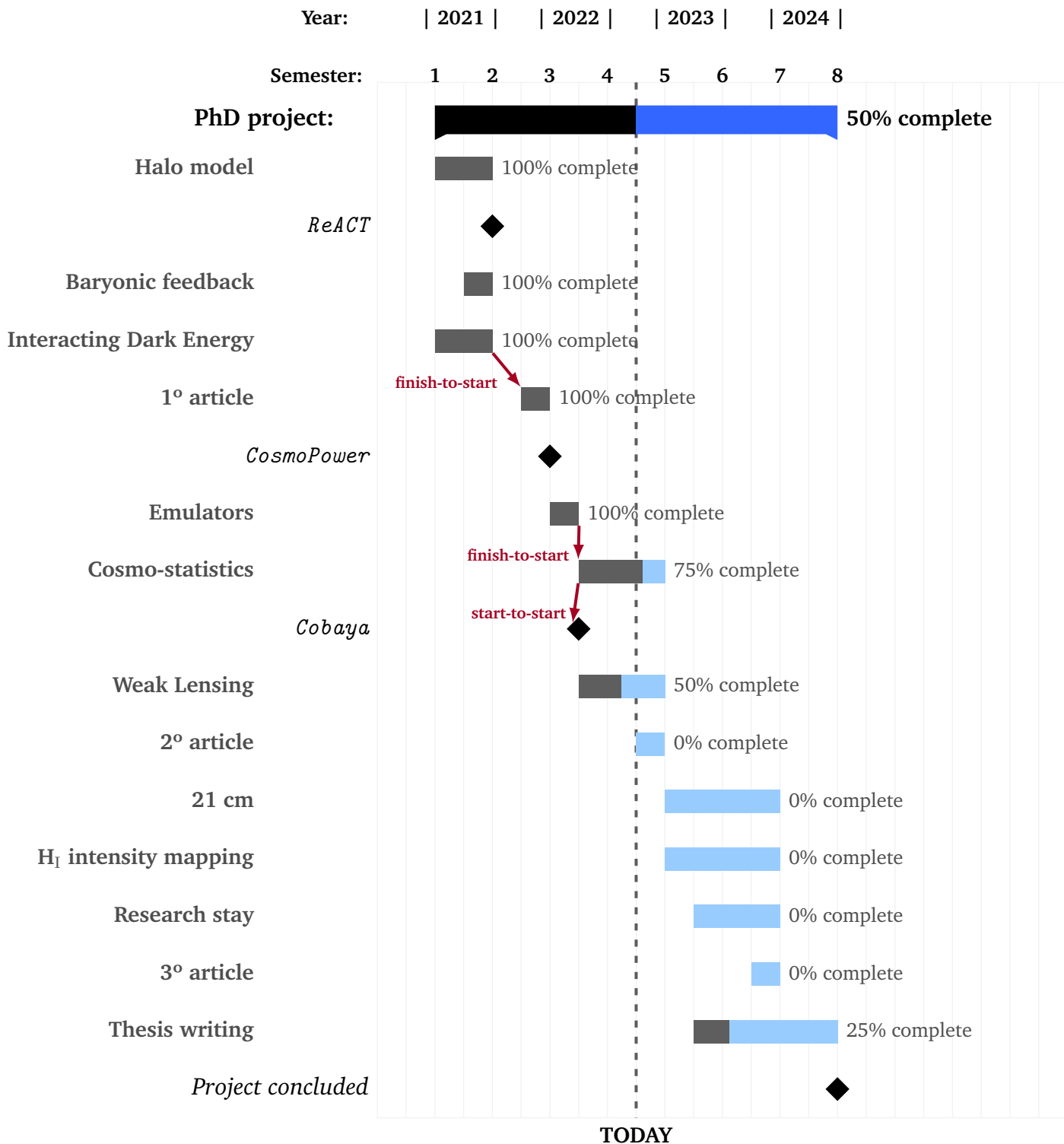


Figure 6.7: Posteriors comparison using the linear power spectrum ($\mathcal{P}_L(k)$) from the CosmoPower Λ CDM emulator and the CLASS prediction matching the year 1 DES data published in [Abbott et al., 2018], via the DES likelihood module in Cobaya .

WORKPLAN

Proposed schedule of activities to complete the project.



References

- Abbott, T. M. C., et al. (2018). Dark Energy Survey year 1 results: Cosmological constraints from galaxy clustering and weak lensing. *Phys. Rev. D*, 98(4), 043526. doi: 10.1103/PhysRevD.98.043526
- Abbott, T. M. C., et al. (2022). Dark Energy Survey Year 3 results: Cosmological constraints from galaxy clustering and weak lensing. *Phys. Rev. D*, 105(2), 023520. doi: 10.1103/PhysRevD.105.023520
- Agarwal, S., & Feldman, H. A. (2011). The effect of massive neutrinos on the matter power spectrum. *Monthly Notices of the Royal Astronomical Society*, 410(3), 1647–1654.
- Aghanim, N., et al. (2020). Planck 2018 results. VI. Cosmological parameters. *Astron. Astrophys.*, 641, A6. ([Erratum: *Astron. Astrophys.* 652, C4 (2021)]) doi: 10.1051/0004-6361/201833910
- Amendola, L., Pettorino, V., Quercellini, C., & Vollmer, A. (2012). Testing coupled dark energy with next-generation large-scale observations. *Physical Review D*, 85, 103008.
- Ashton, G., et al. (2022). Nested sampling for physical scientists. *Nature*, 2. doi: 10.1038/s43586-022-00121-x
- Aviles, A., & Cervantes-Cota, J. L. (2017). Lagrangian perturbation theory for modified gravity. *Phys. Rev. D*, 96(12), 123526. doi: 10.1103/PhysRevD.96.123526
- Baldi, M., & Simpson, F. (2015). Simulating Momentum Exchange in the Dark Sector. *Mon. Not. Roy. Astron. Soc.*, 449(3), 2239–2249. doi: 10.1093/mnras/stv405
- Baldi, M., & Simpson, F. (2017). Structure formation simulations with momentum exchange: alleviating tensions between high-redshift and low-redshift cosmological probes. *Mon. Not. Roy. Astron. Soc.*, 465(1), 653–666. doi: 10.1093/mnras/stw2702
- Bernardeau, F., Colombi, S., Gaztanaga, E., & Scoccimarro, R. (2002). Large scale structure of the universe and cosmological perturbation theory. *Phys. Rept.*, 367, 1–248. doi: 10.1016/S0370-1573(02)00135-7
- Bertolami, O., Carrilho, P., & Paramos, J. (2012). Two-scalar-field model for the interaction of dark energy and dark matter. *Phys. Rev. D*, 86, 103522. doi: 10.1103/PhysRevD.86.103522
- Bose, B., Baldi, M., & Pourtsidou, A. (2018). Modelling Non-Linear Effects of Dark Energy. *JCAP*, 04, 032. doi: 10.1088/1475-7516/2018/04/032
- Bose, B., Cataneo, M., Tröster, T., Xia, Q., Heymans, C., & Lombriser, L. (2020). On the road to per cent accuracy IV: ReACT – computing the non-linear power spectrum beyond Λ CDM. *Mon. Not. Roy. Astron. Soc.*, 498(4), 4650–4662. doi: 10.1093/mnras/staa2696

- Bose, B., Tsedrik, M., Kennedy, J., Lombriser, L., Pourtsidou, A., & Taylor, A. (2022, 10). Fast and accurate predictions of the nonlinear matter power spectrum for general models of Dark Energy and Modified Gravity.
- Bose, B., Wright, B. S., Cataneo, M., Pourtsidou, A., Giocoli, C., Lombriser, L., . . . Xia, Q. (2021). On the road to per cent accuracy – V. The non-linear power spectrum beyond Λ CDM with massive neutrinos and baryonic feedback. *Mon. Not. Roy. Astron. Soc.*, *508*(2), 2479–2491. doi: 10.1093/mnras/stab2731
- Caldera-Cabral, G., Maartens, R., & Urena-Lopez, L. (2009). Dynamics of interacting dark energy. *Phys. Rev. D*, *79*, 063518. doi: 10.1103/PhysRevD.79.063518
- Carrilho, P., Carrion, K., Bose, B., Pourtsidou, A., Hidalgo, J. C., Lombriser, L., & Baldi, M. (2022). On the road to per cent accuracy VI: the non-linear power spectrum for interacting dark energy with baryonic feedback and massive neutrinos. *Mon. Not. Roy. Astron. Soc.*, *512*(3), 3691–3702. doi: 10.1093/mnras/stac641
- Carrilho, P., Moretti, C., Bose, B., Markovič, K., & Pourtsidou, A. (2021). Interacting dark energy from redshift-space galaxy clustering. *JCAP*, *10*, 004. doi: 10.1088/1475-7516/2021/10/004
- Carrilho, P., Moretti, C., & Pourtsidou, A. (2022, 7). Cosmology with the EFTofLSS and BOSS: dark energy constraints and a note on priors.
- Cataneo, M. (2022, 3). On the road to percent accuracy: The Reaction Way. In *56th Rencontres de Moriond on Cosmology*.
- Cataneo, M., Emberson, J. D., Inman, D., Harnois-Deraps, J., & Heymans, C. (2020). On the road to per cent accuracy – III. Non-linear reaction of the matter power spectrum to massive neutrinos. *Mon. Not. Roy. Astron. Soc.*, *491*(3), 3101–3107. doi: 10.1093/mnras/stz3189
- Cataneo, M., Lombriser, L., Heymans, C., Mead, A., Barreira, A., Bose, S., & Li, B. (2019). On the road to percent accuracy: non-linear reaction of the matter power spectrum to dark energy and modified gravity. *Mon. Not. Roy. Astron. Soc.*, *488*(2), 2121–2142. doi: 10.1093/mnras/stz1836
- Chevallier, M., & Polarski, D. (2001). Accelerating universes with scaling dark matter. *Int. J. Mod. Phys. D*, *10*, 213–224. doi: 10.1142/S0218271801000822
- Chisari, N. E., et al. (2019). Modelling baryonic feedback for survey cosmology. *Open J. Astrophys.*, *2*(1), 4. doi: 10.21105/astro.1905.06082
- Cooray, A., & Sheth, R. K. (2002). Halo Models of Large Scale Structure. *Phys. Rept.*, *372*, 1–129. doi: 10.1016/S0370-1573(02)00276-4
- Cunnington, S., Pourtsidou, A., Soares, P. S., Blake, C., & Bacon, D. (2020). Multipole expansion for H I intensity mapping experiments: simulations and modelling. *Mon. Not. Roy. Astron. Soc.*, *496*(1), 415–433. doi: 10.1093/mnras/staa1524
- Di Valentino, E., Melchiorri, A., & Mena, O. (2017). Can interacting dark energy solve the H_0 tension? *Phys. Rev. D*, *96*(4), 043503. doi: 10.1103/PhysRevD.96.043503
- Di Valentino, E., Melchiorri, A., Mena, O., & Vagnozzi, S. (2020). Interacting dark energy in the early 2020s: A promising solution to the H_0 and cosmic shear tensions. *Phys. Dark Univ.*, *30*, 100666. doi: 10.1016/j.dark.2020.100666

- Di Valentino, E., Mena, O., Pan, S., Visinelli, L., Yang, W., Melchiorri, A., . . . Silk, J. (2021). In the realm of the Hubble tension—a review of solutions. *Class. Quant. Grav.*, 38(15), 153001. doi: 10.1088/1361-6382/ac086d
- Dodelson, S., & Schmidt, F. (2020). *Modern cosmology*. Academic Press.
- Douspis, M., Salvati, L., & Aghanim, N. (2018). On the Tension between Large Scale Structures and Cosmic Microwave Background. *PoS, EDSU2018*, 037. doi: 10.22323/1.335.0037
- Ellis, G. F., Maartens, R., & MacCallum, M. A. (2012). *Relativistic cosmology*. Cambridge University Press.
- Gao, L.-Y., Zhao, Z.-W., Xue, S.-S., & Zhang, X. (2021). Relieving the H 0 tension with a new interacting dark energy model. *JCAP*, 07, 005. doi: 10.1088/1475-7516/2021/07/005
- Heymans, C., et al. (2021). KiDS-1000 Cosmology: Multi-probe weak gravitational lensing and spectroscopic galaxy clustering constraints. *Astron. Astrophys.*, 646, A140. doi: 10.1051/0004-6361/202039063
- Kerscher, M., Szapudi, I., & Szalay, A. S. (2000). A Comparison of estimators for the two-point correlation function. *Astrophys. J. Lett.*, 535, L13–L16. doi: 10.1086/312702
- Knabenhans, M., et al. (2021). Euclid preparation: IX. EuclidEmulator2 – power spectrum emulation with massive neutrinos and self-consistent dark energy perturbations. *Mon. Not. Roy. Astron. Soc.*, 505(2), 2840–2869. doi: 10.1093/mnras/stab1366
- Lesgourgues, J. (2011, April). The Cosmic Linear Anisotropy Solving System (CLASS) I: Overview. *arXiv e-prints*, arXiv:1104.2932.
- Lewis, A., Challinor, A., & Lasenby, A. (2000). Efficient computation of CMB anisotropies in closed FRW models. *Astrophys. J.*, 538, 473–476. doi: 10.1086/309179
- Malik, K. A., & Wands, D. (2009). Cosmological perturbations. *Phys. Rept.*, 475, 1-51. doi: 10.1016/j.physrep.2009.03.001
- Mancini Spurio, A., & Pourtsidou, A. (2022). KiDS-1000 cosmology: machine learning – accelerated constraints on interacting dark energy with CosmoPower. *Mon. Not. Roy. Astron. Soc.*, 512(1), L44–L48. doi: 10.1093/mnrasl/slac019
- Massara, E., Villaescusa-Navarro, F., & Viel, M. (2014). The halo model in a massive neutrino cosmology. *JCAP*, 12, 053. doi: 10.1088/1475-7516/2014/12/053
- McCarthy, I. G., Schaye, J., Bird, S., & Le Brun, A. M. C. (2017). The BAHAMAS project: Calibrated hydrodynamical simulations for large-scale structure cosmology. *MNRAS*, 465(3), 2936–2965. doi: 10.1093/mnras/stw2792
- Mead, A., Brieden, S., Tröster, T., & Heymans, C. (2021). Hmcode-2020: Improved modelling of non-linear cosmological power spectra with baryonic feedback. *Monthly Notices of the Royal Astronomical Society*, 502(1), 1401–1422.
- Moresco, M., et al. (2022, 1). Unveiling the Universe with Emerging Cosmological Probes.
- Perepelkin, E., Sadovnikov, B., Inozemtseva, N., & Suchkov, D. (2018). The vlasov equation correct application based on the higher orders kinematic values for the dissipative systems description. *arXiv preprint arXiv:1811.09424*.

- Pourtsidou, A. (2022, 6). Interferometric HI intensity mapping: perturbation theory predictions and foreground removal effects.
- Pourtsidou, A., Skordis, C., & Copeland, E. J. (2013). Models of dark matter coupled to dark energy. *Phys. Rev. D*, *88*(8), 083505. doi: 10.1103/PhysRevD.88.083505
- Pourtsidou, A., & Tram, T. (2016). Reconciling CMB and structure growth measurements with dark energy interactions. *Phys. Rev. D*, *94*(4), 043518. doi: 10.1103/PhysRevD.94.043518
- Riess, A. G. (2019). The Expansion of the Universe is Faster than Expected. *Nature Rev. Phys.*, *2*(1), 10–12. doi: 10.1038/s42254-019-0137-0
- Schmidt, F., Lima, M. V., Oyaizu, H., & Hu, W. (2009). Non-linear Evolution of $f(R)$ Cosmologies III: Halo Statistics. *Phys. Rev. D*, *79*, 083518. doi: 10.1103/PhysRevD.79.083518
- Sheth, R. K., Mo, H. J., & Tormen, G. (2001). Ellipsoidal collapse and an improved model for the number and spatial distribution of dark matter haloes. *Mon. Not. Roy. Astron. Soc.*, *323*, 1. doi: 10.1046/j.1365-8711.2001.04006.x
- Sheth, R. K., & Tormen, G. (1999). Large scale bias and the peak background split. *Mon. Not. Roy. Astron. Soc.*, *308*, 119. doi: 10.1046/j.1365-8711.1999.02692.x
- Simpson, F. (2010). Scattering of dark matter and dark energy. *Phys. Rev. D*, *82*, 083505. doi: 10.1103/PhysRevD.82.083505
- Skordis, C., Pourtsidou, A., & Copeland, E. J. (2015). Parametrized post-Friedmannian framework for interacting dark energy theories. *Phys. Rev. D*, *91*(8), 083537. doi: 10.1103/PhysRevD.91.083537
- Springel, V. (2005). The Cosmological simulation code GADGET-2. *Mon. Not. Roy. Astron. Soc.*, *364*, 1105–1134. doi: 10.1111/j.1365-2966.2005.09655.x
- Spurio Mancini, A., Piras, D., Alsing, J., Joachimi, B., & Hobson, M. P. (2022, Jan). Cosmopower: emulating cosmological power spectra for accelerated bayesian inference from next-generation surveys. *Monthly Notices of the Royal Astronomical Society*, *511*(2), 1771–1788. Retrieved from <http://dx.doi.org/10.1093/mnras/stac064> doi: 10.1093/mnras/stac064
- Tarrant, E. R. M., van de Bruck, C., Copeland, E. J., & Green, A. M. (2012, January). Coupled quintessence and the halo mass function. *Phys. Rev. D*, *85*(2), 023503. doi: 10.1103/PhysRevD.85.023503
- Verde, L., Treu, T., & Riess, A. G. (2019, 7). Tensions between the Early and the Late Universe. *Nature Astron.*, *3*, 891. doi: 10.1038/s41550-019-0902-0
- Yao, Y.-H., & Meng, X.-H. (2022, 7). Can interacting dark energy with dynamical coupling resolve the Hubble tension.